



HAL
open science

Geochemical Characterization of the Oman Crust-Mantle Transition Zone, OmanDP Holes CM1A and CM2B

F. Kourim, M. Rospabé, N. Dygert, S. Chatterjee, E. Takazawa, K. -L. Wang,
M. Godard, Benoit Benoit, M. Giampouras, K. Ishii, et al.

► **To cite this version:**

F. Kourim, M. Rospabé, N. Dygert, S. Chatterjee, E. Takazawa, et al.. Geochemical Characterization of the Oman Crust-Mantle Transition Zone, OmanDP Holes CM1A and CM2B. *Journal of Geophysical Research: Solid Earth*, 2022, 127 (4), 10.1029/2021JB022694 . insu-03668202

HAL Id: insu-03668202

<https://insu.hal.science/insu-03668202>

Submitted on 31 Oct 2022

HAL is a multi-disciplinary open access archive for the deposit and dissemination of scientific research documents, whether they are published or not. The documents may come from teaching and research institutions in France or abroad, or from public or private research centers.

L'archive ouverte pluridisciplinaire **HAL**, est destinée au dépôt et à la diffusion de documents scientifiques de niveau recherche, publiés ou non, émanant des établissements d'enseignement et de recherche français ou étrangers, des laboratoires publics ou privés.

Copyright

JGR Solid Earth

RESEARCH ARTICLE

10.1029/2021JB022694

Special Section:

Ophiolites and Oceanic Lithosphere, with a focus on the Samail ophiolite in Oman

Key Points:

- The transition from the oceanic crust to the mantle of Oman has been drilled in the crust-mantle Holes during Phase 2 of the International Continental Scientific Drilling Project Oman Drilling Project
- There is large petrological and chemical variability in the dunites and harzburgites from Holes CM1A and CM2B
- Partial melting versus melt-rock reaction, and the effects of serpentinization and carbonation of dunites and harzburgites are investigated

Supporting Information:

Supporting Information may be found in the online version of this article.

Correspondence to:

F. Kourim,
k.fatna@gmail.com

Citation:

Kourim, F., Rospabé, M., Dygert, N., Chatterjee, S., Takazawa, E., Wang, K.-L., et al. (2022). Geochemical characterization of the Oman crust-mantle transition zone, OmanDP Holes CM1A and CM2B. *Journal of Geophysical Research: Solid Earth*, 127, e2021JB022694. <https://doi.org/10.1029/2021JB022694>










Received 1 JUL 2021
Accepted 24 DEC 2021

Author Contributions:

Conceptualization: F. Kourim, M. Rospabé, E. Takazawa, M. Godard, M. Benoit, D. A.-H. Teagle, P. Kelemen
Data curation: F. Kourim, M. Rospabé, N. Dygert, S. Chatterjee, E. Takazawa, M. Godard, M. Benoit, M. Giampouras, K. Ishii, D. A.-H. Teagle, M.-J. Cooper, P. Kelemen

© 2022. American Geophysical Union.
All Rights Reserved.

Geochemical Characterization of the Oman Crust-Mantle Transition Zone, OmanDP Holes CM1A and CM2B

F. Kourim¹ , M. Rospabé² , N. Dygert³ , S. Chatterjee⁴ , E. Takazawa⁴,
K.-L. Wang^{1,5} , M. Godard⁶ , M. Benoit⁷, M. Giampouras⁸, K. Ishii⁴, D. A.-H. Teagle⁹ ,
M.-J. Cooper⁹ , and P. Kelemen¹⁰ 

¹Institute of Earth Sciences, Academia Sinica, Taipei, Taiwan, ²Research Institute for Marine Geodynamics (IMG), Japan Agency for Marine-Earth Science and Technology (JAMSTEC), Yokosuka, Japan, ³Department of Earth & Planetary Sciences, University of Tennessee, Knoxville, TN, USA, ⁴Department of Geology, Faculty of Science, Niigata University, Niigata, Japan, ⁵Department of Earth Sciences, National Taiwan University, Taipei, Taiwan, ⁶Géosciences Montpellier, CNRS, Université Montpellier, Montpellier, France, ⁷Géosciences Environnement Toulouse (GET), Observatoire Midi-Pyrénées, Université de Toulouse, CNRS, IRD, Toulouse, France, ⁸Instituto Andaluz de Ciencias de la Tierra (IACT), Consejo Superior de Investigaciones Científicas, Universidad de Granada, Granada, Spain, ⁹School of Ocean & Earth Science, National Oceanography Centre Southampton, University of Southampton, Southampton, UK, ¹⁰Lamont-Doherty Earth Observatory, Columbia University, Palisades, NY, USA

Abstract The transition from the gabbroic oceanic crust to the residual mantle harzburgites of the Oman ophiolite has been drilled at Holes CM1A and CM2B (Wadi Tayin massif) during Phase 2 of the International Continental Scientific Drilling Program Oman Drilling Project (November 2017–January 2018). In order to unravel the formation processes of ultramafic rocks in the Wadi Tayin massif crust-mantle transition zone and deeper in the mantle sections beneath oceanic spreading centers, our study focuses on the whole rock major and trace element compositions (together with CO₂ and H₂O concentrations) of these ultramafic rocks (56 dunites and 49 harzburgites). Despite extensive serpentinization and some carbonation, most of the trace element contents (REE, HFSE, Ti, Th, U) record high temperature, magmatic process-related signatures. Two major trends are observed, with good correlations between (a) Th and U, Nb and LREE on one hand, and between (b) heavy REE, Ti and Hf on the other hand. We interpret the first trend as the signature of late melt/peridotite interactions as LREE are known to be mobilized by such processes (“lithospheric process”) and the second trend as the signature of the initial mantle partial melting (“asthenospheric process”), with little or no overprint from melt/rock reaction events.

Plain Language Summary We focus on the transition from the oceanic crust to the Earth's mantle by studying Holes CM1A and CM2B, drilled in the Oman ophiolite during Phase 2 of the International Continental Scientific Drilling Program Oman Drilling Project. Despite extensive serpentinization and some carbonation, the dunites and harzburgites from the transition zone and the mantle section show a large variability in their petrological and chemical compositions. Results indicate that most of the trace element contents (REE, HFSE, Ti, Th, U) record high temperature, magmatic process-related signatures. Two major trends are observed, with good correlations between (a) Th and U, Nb and LREE on one hand, and between (b) heavy REE, Ti and Hf on the other hand. We interpret the first trend as the signature of late interactions between a percolating melt and the harzburgites and/or dunites, and the second trend as the signature of the initial mantle partial melting, with little or no overprint from melt/rock reaction events.

1. Introduction

Melts play a fundamental role in generating lithospheric mantle chemical and mineralogical heterogeneities, and have a large effect on mantle rheology, viscosity and seismic anisotropy (Batanova & Savelieva, 2009; Kelemen et al., 1997; Tommasi & Vauchez, 2015). Numerous studies have been dedicated to melt-rock interaction characterization in both the continental and the oceanic lithospheric mantle (e.g., Bodinier et al., 1990; Dalton et al., 2017; Dygert et al., 2016; Godard et al., 2008; Kelemen & Ghiorso, 1986; Kelemen et al., 1990, 1998; Morgan et al., 2008; Navon & Stolper, 1987; Niu, 1997; Parkinson & Pearce, 1998; Takazawa et al., 1992; Vauchez et al., 2005; Warren and Shimizu, 2010; Warren et al., 2009). Several studies demonstrated that trace element variations coupled with microstructural, mineralogical and petrological observations, and trace element

Formal analysis: F. Kourim, M. Rospabé, N. Dygert, S. Chatterjee, E. Takazawa, K.-L. Wang, M. Godard, M. Benoit, M. Giampouras, K. Ishii, D. A.-H. Teagle, M.-J. Cooper, P. Kelemen

Funding acquisition: F. Kourim, K.-L. Wang, M. Godard, M. Benoit, D. A.-H. Teagle, P. Kelemen

Investigation: F. Kourim, M. Rospabé, N. Dygert, S. Chatterjee, E. Takazawa, K.-L. Wang, M. Godard, M. Benoit, D. A.-H. Teagle, P. Kelemen

Methodology: F. Kourim, M. Rospabé, N. Dygert, E. Takazawa, M. Godard, M. Benoit, K. Ishii, D. A.-H. Teagle, P. Kelemen

Project Administration: D. A.-H. Teagle, P. Kelemen

Resources: E. Takazawa, K.-L. Wang, M. Godard, M. Benoit, D. A.-H. Teagle, P. Kelemen

Software: F. Kourim, M. Rospabé, N. Dygert, M. Godard, M. Benoit, M. Giampouras, K. Ishii, D. A.-H. Teagle, M.-J. Cooper, P. Kelemen

Supervision: F. Kourim, E. Takazawa, K.-L. Wang, M. Godard, M. Benoit, D. A.-H. Teagle, P. Kelemen

Validation: F. Kourim, M. Rospabé, N. Dygert, E. Takazawa, K.-L. Wang, M. Godard, M. Benoit, M. Giampouras, D. A.-H. Teagle, P. Kelemen

Visualization: F. Kourim, M. Rospabé, K.-L. Wang, M. Godard, M. Benoit, D. A.-H. Teagle, P. Kelemen

Writing – original draft: F. Kourim, M. Rospabé

Writing – review & editing: F. Kourim, M. Rospabé, N. Dygert, S. Chatterjee, E. Takazawa, K.-L. Wang, M. Godard, M. Benoit, D. A.-H. Teagle, P. Kelemen

numerical modeling, are a pertinent way to evaluate melt transport and constrain melt-peridotite processes (e.g., Batanova et al., 1998; Godard et al., 1995; Kelemen & Ghiorso, 1986; Kelemen et al., 1995; Kourim et al., 2014; Navon & Stolper, 1987; Oliveira et al., 2020). Despite all these studies, the nature of melt and/or fluids involved in the reactional processes in the oceanic upper mantle below spreading centers remains debated. One of the biggest challenges to understanding these processes is finding locations where samples that were affected by either incomplete melt extraction or interaction with melt with samples that were not affected by either of these processes. Abyssal peridotites (e.g., Godard et al., 2008; Johnson et al., 1990; Niu, 1997; Parkinson & Pearce, 1998) and mantle xenoliths (e.g., Bedini & Bodinier, 1999; Dalton et al., 2017; Fitzpayne et al., 2018; Grégoire et al., 2001) are good candidates to study mantle processes in present-day oceanic and continental settings, but their sampling is sparse, lacking second-order geologic context and is limited to the uppermost oceanic and continental mantle.

Oman ophiolite has been instrumental in elucidating the accretion and evolution of oceanic lithosphere in present-day oceans and exhibits the largest ophiolitic exposures of oceanic lithosphere worldwide. The mantle section of the Oman ophiolite is mainly composed of depleted harzburgites and of some dunites, and has been the subject of many petrological, geochemical and structural studies (e.g., Boudier & Coleman, 1981; Ceuleneer et al., 1988; Dygert et al., 2017; Godard et al., 2000; Kelemen et al., 1995; Le Mée et al., 2004; Monnier et al., 2006; Nicolas et al., 2000; Takazawa et al., 2003). The general consensus stands that the dunites, as channels in the mantle section or massive at the crust-mantle transition, are residues of reaction between a melt undersaturated in silica at low pressure and mantle harzburgites; this reaction leads to the complete consumption of orthopyroxene (opx) and to the concomitant precipitation of Olivine (ol) (e.g., Abily & Ceuleneer, 2013; Boudier & Nicolas, 1995; Braun & Kelemen, 2002; Godard et al., 2000; Kelemen et al., 1995, 1997; Koga et al., 2001; Quick, 1981a; Rabinowicz et al., 1987; Rospabé et al., 2017, Rospabé, Benoit, & Candaudap, 2018, Rospabé, Benoith et al., 2019). However, the relationship between the harzburgites and the dunites, the nature of the reactant melt, and the chemical budgets related to the “dunitization” process itself, are still debated. Oman ophiolite exposes large portions of the mantle and crust-mantle transition zone (CMTZ), suitable to understanding local to large scale studies of mantle heterogeneities and melt/peridotite reaction processes. The Oman Drilling Project (OmanDP) enabled sampling of a continuous section of the crust-mantle transition at Holes CM1A and CM2B (Wadi Tayin Massif, during Phase two of the International Continental Scientific Drilling Project (ICDP) OmanDP, November 2017–January 2018), starting from the base of the layered gabbroic crust and going through the uppermost harzburgitic mantle (Kelemen et al., 2020a, 2020b; Proceedings available at <https://www.omandrilling.ac.uk/>). In this paper, we characterize the major and trace element contents of the dunites and harzburgites from the Hole CM1A and CM2B drill cores to better constrain dunitization processes by first, gaining insights into Wadi Tayin mantle and crust-mantle geochemical characteristics, then, comparing these characteristics to previously studied Maqsd diapir harzburgites and mantle-crust transition zone, taking advantage of the continuous and regular, high resolution sampling performed in the OmanDP.

2. Geological Setting and Context of CM Drill Cores

2.1. Geology of the Samail Ophiolite

The Samail ophiolite, located in the Sultanate of Oman and the United Arab Emirates (Figure 1a), exposes a relatively continuous section of oceanic lithosphere, with, from top-to-depth, a 5–7 km-thick crust made of pillow basalts, a sheeted dike complex and gabbros, overlying the crust-mantle transition at the top of the upper mantle peridotites (e.g., Glennie et al., 1974; Hopson et al., 1981; Lippard et al., 1986; Nicolas, 2012; Nicolas et al., 1988; Searle & Malpas, 1980 and references therein). According to the ages of pelagic sediments interbedded with basalts and of zircons in evolved gabbroic and plagiogranitic rocks, the accretion event that led to the formation of the Oman ophiolite has been estimated at around 94–97 Ma ago (Rioux et al., 2012, 2013, 2016; Tilton et al., 1981; Tippit et al., 1981; Warren et al., 2005). The tectonic setting in which the Samail ophiolite evolved is still debated. The spatial distribution along the ophiolite of the nature of the (a) mafic dikes cutting-across the mantle section, and (b) lower crustal cumulates, as well as their geochemical signature, attest that both MORB like and depleted calc-alkaline series coexisted during the igneous evolution of the ophiolite (e.g., Benoit et al., 1999, 1996; Ceuleneer et al., 1996; Clénet et al., 2010; Python & Ceuleneer, 2003; Python et al., 2008). The dikes belonging to the MORB-like volcanic units have been mapped mainly in the SE of the ophiolite and in other more restricted spots, whereas the depleted calc-alkaline series were observed at a more widespread scale (Python & Ceuleneer, 2003).

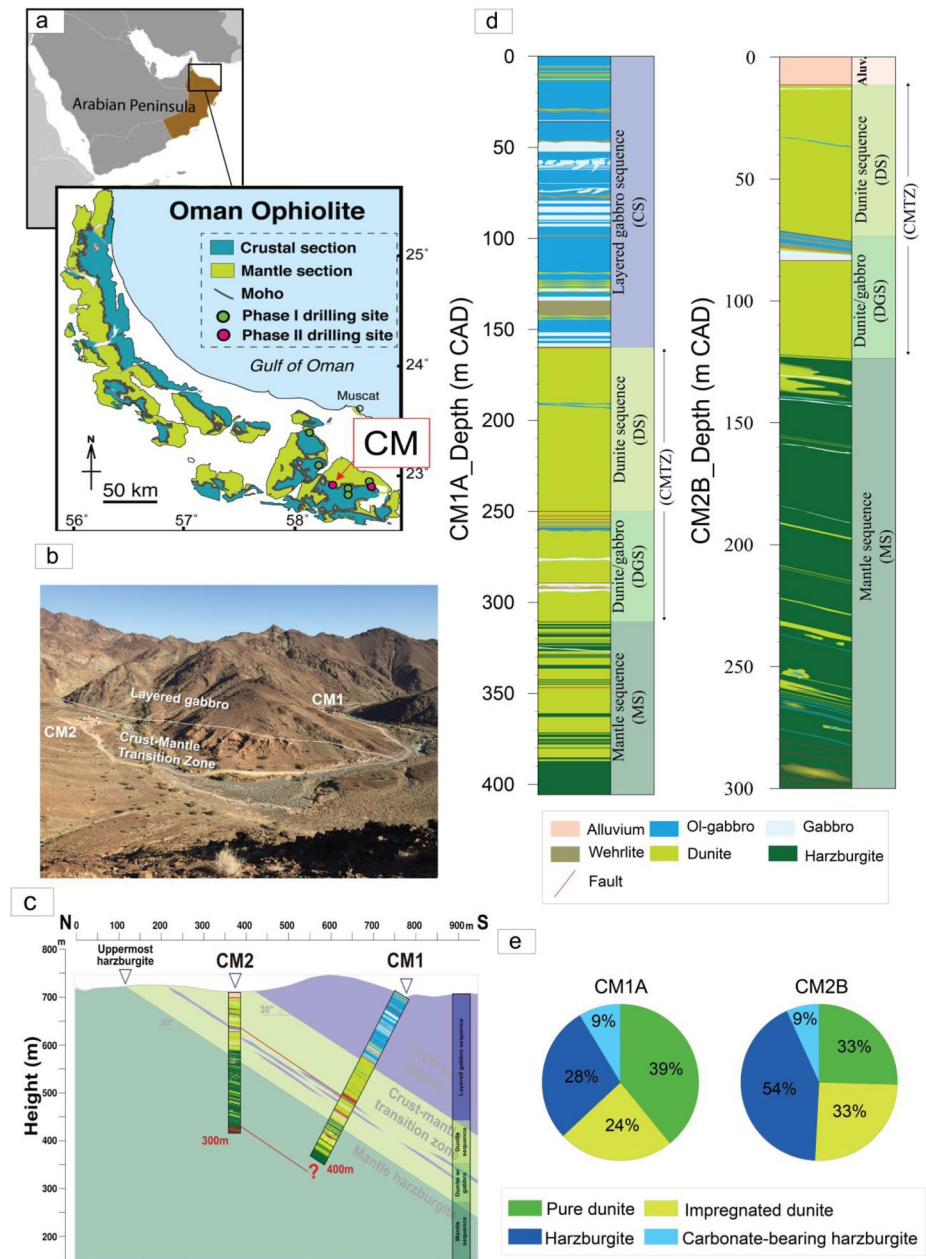


Figure 1. Geological context, (a) Simplified geological map showing the location of Holes CM1A and CM2B in the context of the regional and local geology (after Nicolas & Boudier, 1995). (b) Field photographs showing the location of Holes CM1A and CM2B. (c) Simplified N-S cross-section showing the different sampled lithologies and the correlation in depth between Holes CM1A and CM2B (d) Downhole stratigraphy of CM1A and CM2B showing the distribution of the lithologies in the crust, crust-mantle and mantle sequences. (e) pie charts showing the studied samples lithology count in Hole CM1A and CM2B (see Section 3 in the Supporting Information S1).

Along the Samail ophiolite, spatially constrained vertical flow structures frozen within the mantle section were interpreted as former asthenospheric diapirs distributed along the oceanic ridge (Ceuleneer, 1991; Ceuleneer et al., 1988; Joussetin et al., 1998; Nicolas et al., 1988, 2000). This mantle section is mainly composed of harzburgites (85%–95%), relatively depleted with a typical opx content of 15%–25% and locally grading into lherzolites, and to a lesser extent of dunites (5%–15%; Boudier & Coleman, 1981; Lippard et al., 1986). The crust-mantle transition is mainly made of dunites and wehrlites and its thickness varies from a few meters to a few hundred

meters (e.g., Abily & Ceuleneer, 2013; Boudier & Nicolas, 1995; Ceuleneer & Nicolas, 1985; Joussetin & Nicolas, 2000; Koga et al., 2001; Rospabé et al., 2017, Rospabé, Benoit, & Candaudap, 2018).

Geochemical studies have demonstrated the overprint of partial melting and of melt/peridotite reaction processes in the mantle harzburgites' signatures (Gerbert-Gaillard, 2002; Girardeau et al., 2002; Godard et al., 2000; Hanghøj et al., 2010; Kanke & Takazawa, 2014; Khedr et al., 2014; Le Mée et al., 2004; Monnier et al., 2006; Takazawa et al., 2003). In this context, mantle dunites and dunites from the CMTZ have mostly been interpreted as replacive in origin, products of melt-harzburgite reaction leading to the complete consumption of opx and concomitant precipitation of ol (e.g., Abily & Ceuleneer, 2013; Boudier & Nicolas, 1995; Gerbert-Gaillard, 2002; Godard et al., 2000; Kelemen et al., 1997, 1995; Koga et al., 2001; Rabinowicz et al., 1987; Rospabé, Benoit, & Candaudap, 2018). This dunitization process may have been enhanced by the involvement of a hydrous component in the reaction (Rospabé et al., 2017, Rospabé, Benoit, & Candaudap, 2018; Rospabé, Benoit et al., 2019). However, a reaction origin and a cumulate origin are not mutually exclusive as it has been shown that the uppermost part (~20%) of the crust-mantle transition may have a composition consistent with cumulates while the main lower part (~80%) has a composition supporting the replacive origin (Abily & Ceuleneer, 2013). Furthermore, as ol-saturated melt begins to cool conductively, hybrid processes, termed "relative crystallization" (Collier & Kelemen, 2010) produce reactive characteristics (e.g., Abily & Ceuleneer, 2013; Benn et al., 1988; Boudier & Nicolas, 1995; Koga et al., 2001; Rospabé, Benoit, & Candaudap, 2018).

2.2. The Crust-Mantle Transition at Sites CM1 and CM2

Samples studied in this paper were drilled in the Wadi Tayin massif in the SE of the ophiolite during Phase two of the ICDP OmanDP (November 2017–January 2018). According to structural and petrological maps (Gerbert-Gaillard, 2002; Nicolas et al., 2000; Python & Ceuleneer, 2003), this site is located near the border - or in an intermediate position between the border and the axis of the frozen paleo-spreading center centered on the Maqsad (Sumail massif) paleo-mantle diapir - of the MORB segment in this part of the ophiolite. The CMTZ is relatively well exposed in this area, with a clear transition from harzburgite to the north to dunites then gabbros to the south (Figure 1b). The two sites CM1 and CM2, separated by about 400 m, have been drilled twice: with one Hole for core recovery and a second wider Hole for geophysical logging. At these sites 400 m of core was recovered from CM1A and about 300 m of core was recovered from CM2B.

The geological map produced by the OmanDP group during the preparation of Phases 1 and 2 shows a general tilt of the units by about 30° to the south (Figure 1c). Considering these petrological and structural configurations, Hole CM1A borehole was cored 400 m with an inclination of 60° trending to the north, in order to cut perpendicularly across the mantle-crust transition (Figure 1d). It crosses from the gabbroic lower crust (~150 m; the Layered Gabbro "Crustal Sequence", CS), through the dunite-rich CMTZ (~150 m CMTZ) that includes the Dunite (DS) and Dunite with Gabbro Sequences (DGS), to the residual upper mantle harzburgites (~100 m, Mantle Sequence, MS). At Site CM2, the fully cored borehole CM2B is vertical, parallel to the wider rotary borehole for geophysical logging (Hole CM2A). Hole CM2B starts within the CMTZ (~110 m) and extends deeper in the underlying residual mantle peridotites than Hole CM1A (~180 m; Figure 1d). The main rock types sampled in Holes CM1A and CM2B are ol-gabbro, gabbro, dunite, harzburgite and wehrlite, associated with minor gabbronorite, troctolite, websterite, anorthosite, and chromitite layers (Figure 1d). The CMTZ sampled in Hole CM1A and CM2B has been divided into two parts according to the rock types present: the upper half is mainly made of dunites containing rare melt migration features (DS for Dunite Sequence); in the lower half, the dunites alternate with thin bands containing a higher proportion of interstitial plagioclase (pl) (+/- clinopyroxene), which has been called the DGS. In the present article we focus on the geochemical compositions of dunites from the CS, CMTZ and MS and of mantle harzburgites.

3. Results

The sample selection strategy and the analytical methods are detailed in Supporting Information (see also Kelemen et al., 2020a, 2020b; 2020c). In summary, one sample was taken every 10 m along Holes CM1A and CM2B to cover the entire crust-mantle transition and mantle sections. Additional samples were collected to better characterize some specific levels (e.g., to document local, minor lithologies). The samples were analyzed for their major (as well as volatile) and trace element compositions. Sample lithology, macroscopic and microscopic

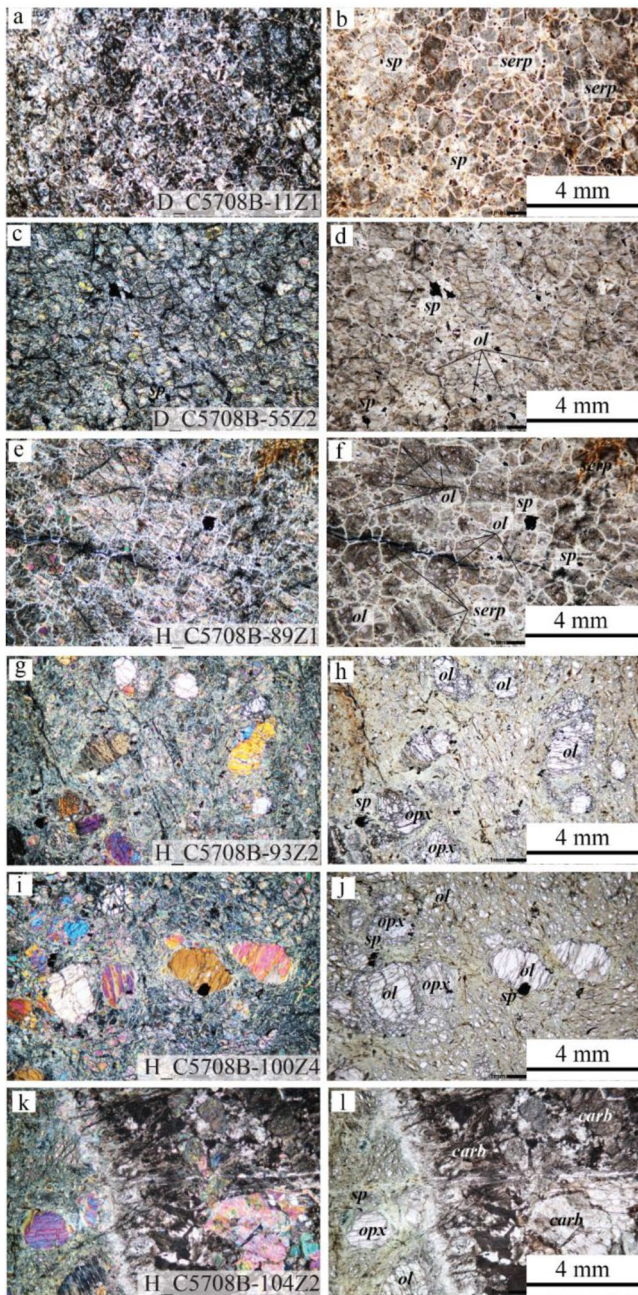


Figure 2. Microphotographs of petrographic details of a selection of crust-mantle transition zone dunites (a, b, c and d) and harzburgites (e, f, g, h, i, j, k and l) from Holes CM1A and CM2B. The dunites are characterized by fine-to medium grained granular texture and the harzburgites by porphyroclastic texture. The dunites and harzburgites have generally preserved their primary high temperature texture (granular or porphyroclastic textures) after complete (a, and b), or partial (c, d, e, f, g, h, i, j, k and l) replacement of olivine crystals by serpentine. i and j illustrate microphotographs of a plastically deformed orthopyroxene surrounded by neoblasts. k and l show harzburgite CM2B-104Z2 crosscut by low-temperature veins (Carbonate).

observations and mineral modes calculated from major elements are reported in Table S1. Whole rock major and volatile element compositions are reported in Table S2. Whole rock trace element compositions are reported in Table S3.

3.1. Sample Description

The studied samples represent the ultramafic lithologies (harzburgites and dunites) of the mantle section (46 harzburgites and 12 dunites), the CMTZ (45 dunites) and the crustal Layered Gabbro Sequence (LGS; 2 dunites) drilled at Holes CM1A (46 samples) and CM2B (59 samples). Lithological classifications were made based on macroscopic and microscopic observations, and mineral modes calculated from XRF measurements (Table S1). Four rock groups have been defined, harzburgites (36), Carbonate (carb)-bearing harzburgites (8), pure dunites (31) and impregnated dunites (29; Figure 1e, Figure SD-1 in Supporting Information S1, Table S1).

The harzburgites and carb-bearing harzburgites contain ol, opx and minor spinel (sp) as primary minerals (Figures 2e–2l, Figure SD-1 in Supporting Information S1, Table S1), displaying a porphyroclastic texture. Ol abundance (primary mode) ranges from 72% to 93% in the harzburgites and from 64% to 75% in carb-bearing harzburgites. The ol typically show subhedral shape and equant habits. Opx abundance ranges from 10% to 28% with mostly subhedral shapes; some opx show sigmoidal crystal-plastic deformation features (Figures 2i and 2j). Grains of spinel are present in all samples (up to 1%–3%). Compared to the dunites, the harzburgites are less altered, the alteration becoming complete only in highly veined zones and at the bottom of both Holes where carb/serpentine (serp) associations occur (Figures 2k and 2l). The most abundant minerals in the harzburgite background alteration are serp and magnetite (mag). The carb alteration occurs at the bottom of both Holes starting at 388.3 m depth in CM1A and at 279.5 m depth in CM2B. Harzburgite sample CM2B 129Z1 5–10 cm (depth 299.7 m) is the most carb vein-rich harzburgite. Secondary amphibole (amph), chlorite and hydrogrossular are also present as trace alteration minerals (abundance <3%, Table S1). No patch or deformation features specifically related to the alteration were observed.

The pure dunites are primarily composed of ol >97% and generally contain <1% sp (Figures 2a–2c and 2d, Table S1). Mineral modes calculated using bulk rock data (Figure SD-1 in Supporting Information S1, Table S1) indicate that many dunites have >10% normative pyroxene. The macroscopic and microscopic descriptions indicate that some dunites contain pl and/or pyroxenes. We refer to this group of dunites as “impregnated dunites” in contrast to the pure dunites containing only ol and sp. The ol in almost all samples has been completely replaced by serp (Figures 2a–2c and 2d). In many dunites and in impregnated dunites, no relics of porphyroclastic opx are present, indicating no textural relics of a porphyroclastic texture. The pure and impregnated dunites’ primary texture was a fine-to medium-grained granular microstructure, characterized by euhedral ol forming a mosaic of equigranular grain size distribution as preserved by the equant contacts between serp mesh cores (Figures 2a–2c and 2d). Alteration minerals mainly consist of serp and mag (Figures 2a–2c and 2d). In addition, brucite (brc) after ol was detected by X-Ray Diffraction (XRD, performed during the ChikyuOman 2018 Leg 3) in some serpentinized dunites from the CMTZ

and in dunites from the mantle sequence (absent in harzburgites). Where relics of ol are present, in rare cases, they are surrounded by serp and mag. If ol is completely serpentinized, the mesh cores are mainly composed of

serp with minor mag and accessory grains of sulfides (These sulfides are equant and anhedral, they have grain sizes of 0.1–1 mm, modes of 0.5%, and are very rich in Ni, Kelemen et al., 2020a, 2020b - see also Lorand, 1988 for an article dedicated to the study of sulfides in Oman peridotites). Serp and more abundant mag at mesh rims trace former ol grain and sub-grain boundaries (Figures 2a–2c and 2d).

3.2. Loss on Ignition, CO₂ and H₂O Contents

Samples from Holes CM1A and CM2B display high loss on ignition (LOI) values. The LOI varies from 8.29 to 14.92 wt.% in the harzburgites, from 9.02 to 23 wt.% in the carb-bearing harzburgites, from 10.14 to 15.31 in the pure dunites and from 6.14 to 15.53 wt.% in the impregnated dunites (Figure 3 and Table S2). The averaged H₂O concentration is 12.0 ± 1.7 wt.% in harzburgites, 11.0 ± 5.5 wt.% in carb-bearing harzburgites, 14.3 ± 1.2 wt.% in dunites and 13.7 ± 1.6 wt.% in impregnated dunites. The LOI values correlate with measured water concentration (H₂O), which slightly decreases downhole (Figure 3). The concentrations of CO₂ measured in harzburgites, carb-bearing harzburgites excluding the carb vein-rich harzburgite CM2B 129Z1 5–10 cm (depth 299.7 m, CO₂ = 19.54 wt.%), pure dunites and impregnated dunites vary from 0.12 to 0.31 wt.%, from 0.36 to 1.30 wt.%, from 0.13 to 0.34 wt.% and from 0.03 to 0.41 wt.% respectively. The averaged CaCO₃ concentration excluding the carb-rich harzburgite mentioned previously (22.77 wt.%), is 0.40 wt.% in harzburgites, 1.57 wt.% in carb-bearing harzburgites, 0.51 wt.% in pure dunites and 0.46 wt.% in impregnated dunites. The downhole profile of CaCO₃ shows an increase in concentration in the deepest part of Holes CM1A and CM2B, with recovered harzburgites having higher CO₂ concentrations, LOI and H₂O contents, consistent with the particularly high alteration degree and high carb content in these samples (serp, brc, carb, see Figure 3 XRD).

3.3. Whole Rock Major Element Compositions

Major element analyses were performed on 36 harzburgites, 8 carb-bearing harzburgites, 31 pure dunites, and 29 impregnated dunites sampled along Holes CM1A and CM2B.

3.3.1. The Mantle Section Sequence (MS)

Harzburgite is the most abundant lithology in the MS (36 harzburgites analyzed) followed by impregnated dunite (9 impregnated dunites analyzed) and pure dunite (4 pure dunites analyzed). Mg# (Mg# = 100 × molar Mg / (Mg + Fe_{total})) in mantle harzburgites is between 90.7 and 92.4. CaO, Al₂O₃, and TiO₂ contents range from 0.19 to 2.07 wt.%, 0.53–0.91 wt.%, and 0.02–0.04 wt.%, respectively (Figure 4). Harzburgite with dunite patches contains lower CaO concentrations than the average value (0.30–0.81 wt.%). Carb-bearing harzburgites are characterized by similar Mg#, Al₂O₃, and TiO₂ contents (90.6, 0.70 wt.% and 0.03 wt.% on average respectively), and very high CaO concentrations ranging from 0.68 to 5.42 wt.% compared to carb-free harzburgites. Dunites from the MS have high Mg#, on average 90.2 for pure dunites and 91.1 for impregnated dunites (Figure 4). The pure dunites have CaO, Al₂O₃ and TiO₂ contents from 0.30 to 0.94 wt.%, 0.32–0.72 wt.%, and 0.02–0.05 wt.% respectively, where the impregnated dunites have CaO contents ranging from 0.14 to 1.59 wt.%, Al₂O₃ from 0.21 to 0.95 wt.% and TiO₂ from 0.02 to 0.04 wt.% (Figure 4). Along the MS, TiO₂ and Al₂O₃ contents do not show any systematic variation with depth. On the other hand, the CaO content shows some variations downhole. The vertical evolution of the CaO content in harzburgites from Hole CM1A is different from other elements; successive trends of increasing and decreasing CaO with depth form a well-defined zigzag pattern. In detail, it increases from 0.97 to 2.1 wt.% between 311 and 340 m and from 0.54 to 1.8 wt.% between 360 and 388 m, and decreases from 2.1 to 0.54 wt.% between 340 and 360 m then from 1.8 to 0.8 wt.% at most from 388 to around 400 m. CaO contents in dunites and nearby harzburgites are correlated. Downhole intervals with the highest CaO contents are characterized by high carb vein concentrations (Figure 3 XRD, and Figure 4).

3.3.2. The Crust-Mantle Transition Zone Sequence (CMTZ)

The CMTZ is composed mainly of pure and impregnated dunites (Figure 1d). 27 pure dunites and 18 impregnated dunites from Holes CM1A and CM2B CMTZ were analyzed. Both pure and impregnated dunites from the CMTZ display slightly lower Mg# (89.9 on average, Figure 4) and CaO concentrations (pure dunites = 0.16 wt.%, and impregnated dunites = 0.28 wt.% on average, Figure 4) compared to the dunites from the MS. Some dunites from CM1A DGS (between 252.96 and 271.42 m) display lower Mg# (Mg# = 86.8–88.0) that seems mostly controlled by the increase in the FeO content. The TiO₂ contents in pure and impregnated dunites from

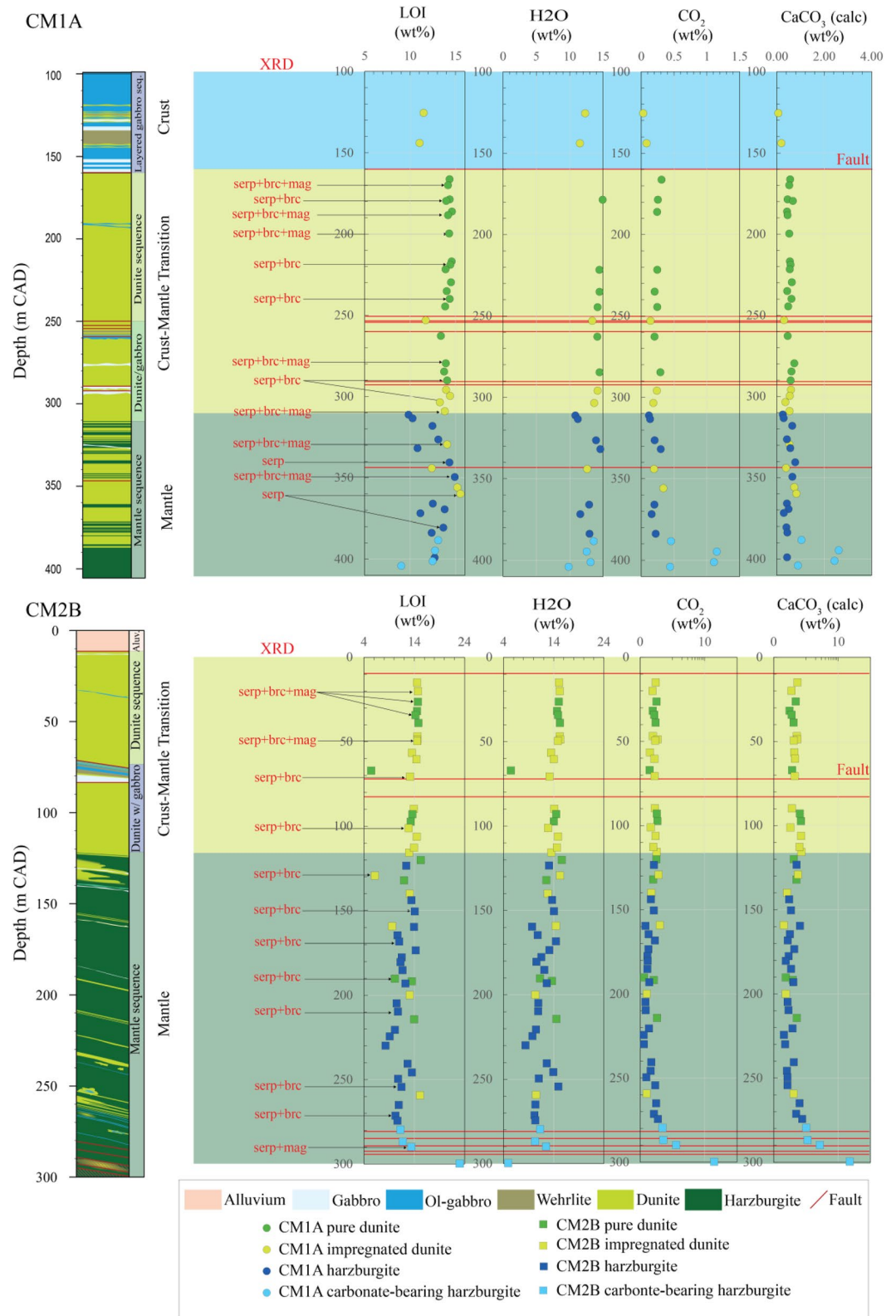


Figure 3. Downhole plots of (from left to right) the lithology, loss on ignition (wt.%), H₂O (wt.%), CO₂ (wt.%) and calculated CaCO₃ (wt.%) contents in pure dunites, impregnated dunites, harzburgites and carbonate-bearing harzburgites recovered samples at Holes CM1A and CM2B. The thick solid red lines indicate the faults. X-Ray Diffraction, serpentine, brucite, magnetite.

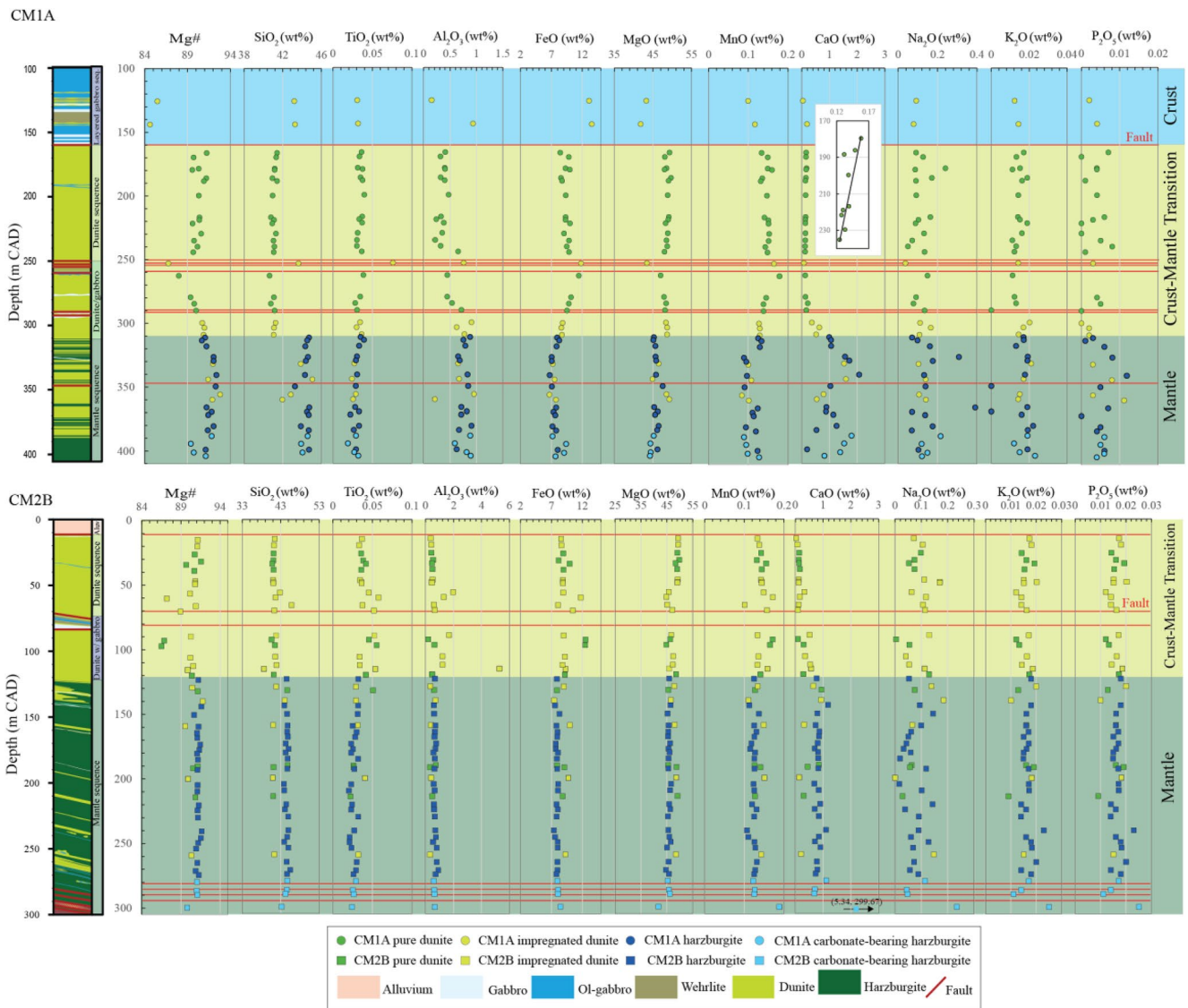


Figure 4. Downhole plots of (from left to right) the lithology, Mg# (cationic $100 \times \text{Mg}/(\text{Mg} + \text{Fe}_{\text{total}})$; calculated assuming all Fe as FeO) (mol%), SiO₂ (wt.%), TiO₂ (wt.%), Al₂O₃ (wt.%), FeO (wt.%), MgO (wt.%), MnO (wt.%), CaO (wt.%), Na₂O (wt.%), K₂O (wt.%), and P₂O₅ (wt.%) in whole rock samples recovered at Holes CM1A and CM2B. The thick solid red lines indicate the faults.

the CMTZ (0.04 wt.% on average) are slightly higher than the TiO₂ contents in the MS dunites (0.03 wt.% on average). Al₂O₃ concentrations are lower in CMTZ pure dunites (0.42 wt.% on average) and higher in impregnated dunites (1.12 wt.% on average) compared to pure (0.53 wt.% on average) and impregnated (0.51 wt.% on average) dunites respectively from the MS. A similar zigzag pattern to the one observed in CaO along the MS is irregularly observed in CMTZ dunites (i.e., in CM1A, decreasing from 0.17 to 0.12 wt.% between 170 and 245 m and, increasing from 0.08 to 0.52 wt.% between 253 and 310 m, Figure 4). This CaO zigzag variation in CM1A CMTZ dunites is associated with Mg# zigzag variation (decreasing from 91 to 89 wt.% between 170 and 245 m and, increasing from 87 to 91 wt.% between 253 and 310 m, Figure 4). The dunites' CaO varies over ~20 m at the base of the CMTZ following the mantle harzburgites zigzag variation, whereas the Mg# varies over ~60 m, along with the FeO variations.

3.3.3. The Crustal Sequence (CS)

The two analyzed dunites from the (LGS; C5707 A-51Z-1 W, 31.0–39.0 cm, 125.60 m in depth, and C5707 A-58Z-2 W, 1.0–6.0 cm, 143.93 m in depth) are impregnated (Figure 4), they have relatively low Mg#

(85.6 and 85.5 respectively), compared to dunites in the other sequences. This tendency is similar to the dunites from CM1A DGS. CaO (0.04 wt.% and 0.19 wt.% respectively), Al₂O₃ (0.15 wt.% and 0.93 wt.% respectively) and TiO₂ (0.03 wt.%) contents are similar to the impregnated dunites values from the MS and the CMTZ (Figure 4).

CM Holes harzburgites, carb-bearing harzburgites, pure dunites and impregnated dunites (except CM1A LGS impregnated dunites) show comparable major element compositions to previously reported harzburgites, dunites and impregnated dunites from the Oman ophiolite mantle and CMTZs (Figure 5). Most of the pure and impregnated dunites from MS, and CMTZ plot above the terrestrial array (Earth differentiation trend, Jagoutz et al., 1979) in the MgO/SiO₂ versus Al₂O₃/SiO₂ diagram, similar to previously studied dunites and impregnated dunites from the mantle section of Wadi Tayin massif (Godard et al., 2000; Hanghøj et al., 2010) and the CMTZ at the top of Maqsd diapir (Rospabé, Benoit, & Candaudap, 2018; Rospabé, Benoit et al., 2019; Figure 5a). Whereas the harzburgites, carb-bearing harzburgites and some pure and impregnated dunites plot below. The MgO-FeO variations in most of the CM dunites mimic the stoichiometric variation of the ol Mg-Fe composition, similar to other pure/slightly impregnated dunites elsewhere, while only a few CM samples fall in the domain of the more highly impregnated dunites. Lower CaO and wider range of Al₂O₃ values characterize all the dunites compared to the harzburgites (Figure 5). Similar to other previously studied Wadi Tayin massif and Maqsd diapir harzburgites (Godard et al., 2000; Hanghøj et al., 2010; Monnier et al., 2006) and most refractory abyssal peridotites (Godard et al., 2008; Niu, 1997; Warren et al., 2009), CM harzburgites plot near the most depleted end of the mantle fractionation array (Figure 5a). They display similar low Al₂O₃/SiO₂ ratios in comparison to other harzburgites from Wadi Tayin and Maqsd harzburgites (0.01–0.02, 0.01–0.04 and 0.01–0.08 respectively), and a high MgO/SiO₂ ratios typical of refractory peridotites (0.98–1.10, 0.95–1.10 and 0.96–1.15 respectively). Oman harzburgites are characterized by narrow FeO and MgO contents compared to the pure and impregnated dunites (Figure 5b), with slightly higher Mg# in CM harzburgites (90.7–92.4) compared to Wadi Tayin and Maqsd harzburgites (89.6–91.5 and 88.4–91.1 respectively). Generally, Al₂O₃ and CaO show broad positive correlation in harzburgites from Wadi Tayin massif and Maqsd diapir (Figures 5c) and Godard et al. (2000) demonstrating that the observed Al₂O₃/CaO ratio variability displayed by Wadi Tayin and Maqsd harzburgites decreases with increasing cpx content in the main harzburgites sequence to lower values in the *cpx*-harzburgites at the base of the mantle section. Al₂O₃/CaO ratio variability is also observed along cores CM1A and CM2B, however CaO variability at the bottom of CM Holes is related to CO₂-bearing fluids interactions with CM harzburgites (see Section 4.1).

3.4. Whole Rock Trace Element Contents

Chondrite-normalized Rare Earth Element (REE) and primitive mantle (PM)-normalized trace element variations and patterns are shown in Figures 6 and 7 respectively. Similar to other refractory peridotites from the Oman ophiolite mantle section and crust-mantle transition, the studied harzburgites, carb-bearing harzburgites, pure dunite and impregnated dunite whole rock concentrations are lower than chondritic (CN) and PM values (Figures 6 and 7). Their REEs are characterized by three types of chondrite-normalized patterns: linear or flat linear, U- or V-shaped, and concave-upward patterns. CM Holes show vertical trends, continuous over tens of meters, in their REE content. These are characterized by ~50 m-thick alternations between increasing and decreasing concentrations (“zigzag” patterns; e.g., La, Yb, LREE patterns; Figure 6). These trends along CM Holes are observed in both dunites and harzburgites, independent of the lithology, and the changes from one trend to another are commonly correlated with the presence of faults described by the structural team during the ChikyuOman2018 Leg 3 (Kelemen et al., 2020a, 2020b).

3.4.1. The Mantle Section Sequence

The mantle harzburgites show two types of chondrite-normalized REE patterns: (a) 19 harzburgites display linear REE patterns characterized by a progressive depletion from heavy REE (HREE; Gd_{CN}/Yb_{CN} = 0.25 ± 0.21, Yb_{CN} = 0.22 ± 0.11) to middle REE (MREE: Sm, Eu and Gd; Sm_{CN} = 0.06 ± 0.05 and Gd_{CN} = 0.06 ± 0.05) and light (LREE; La_{CN}/Sm_{CN} = 0.98 ± 0.74, La_{CN} = 0.06 ± 0.05). Six samples show a positive Eu anomaly ((Eu/Eu*)_{CN} = 2.36 ± 0.66, with (Eu/Eu*)_{CN} = Eu_{CN}/√(Sm_{CN} × Gd_{CN})). In detail, 12 harzburgites display linear LREE-depleted patterns (3 from CM1A and 9 from CM2B) characterized by a progressive depletion from HREE to LREE, and 7 harzburgites (5 from CM1A and 2 from CM2B) display flat linear REE patterns characterized by slightly lower LREE concentrations compared to HREE concentrations. (b) 15 harzburgites (4 from CM1A and 11 from CM2B) display U- or V-shaped REE patterns reflecting significant MREE depletion relative to LREE

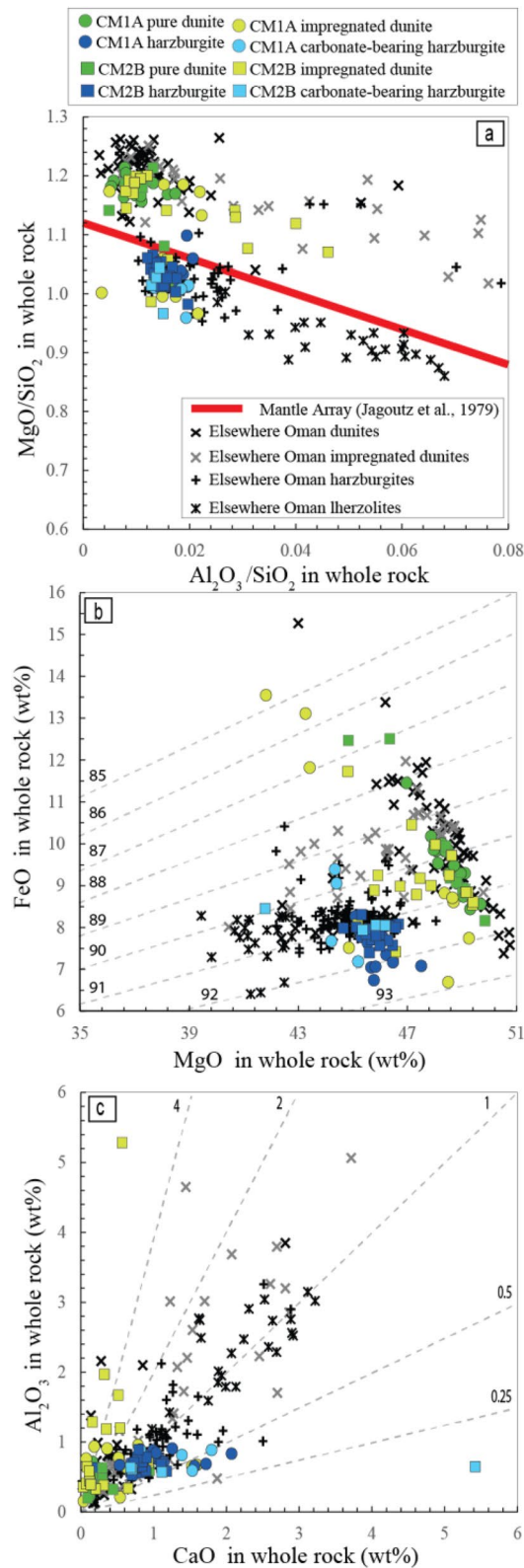


Figure 5.

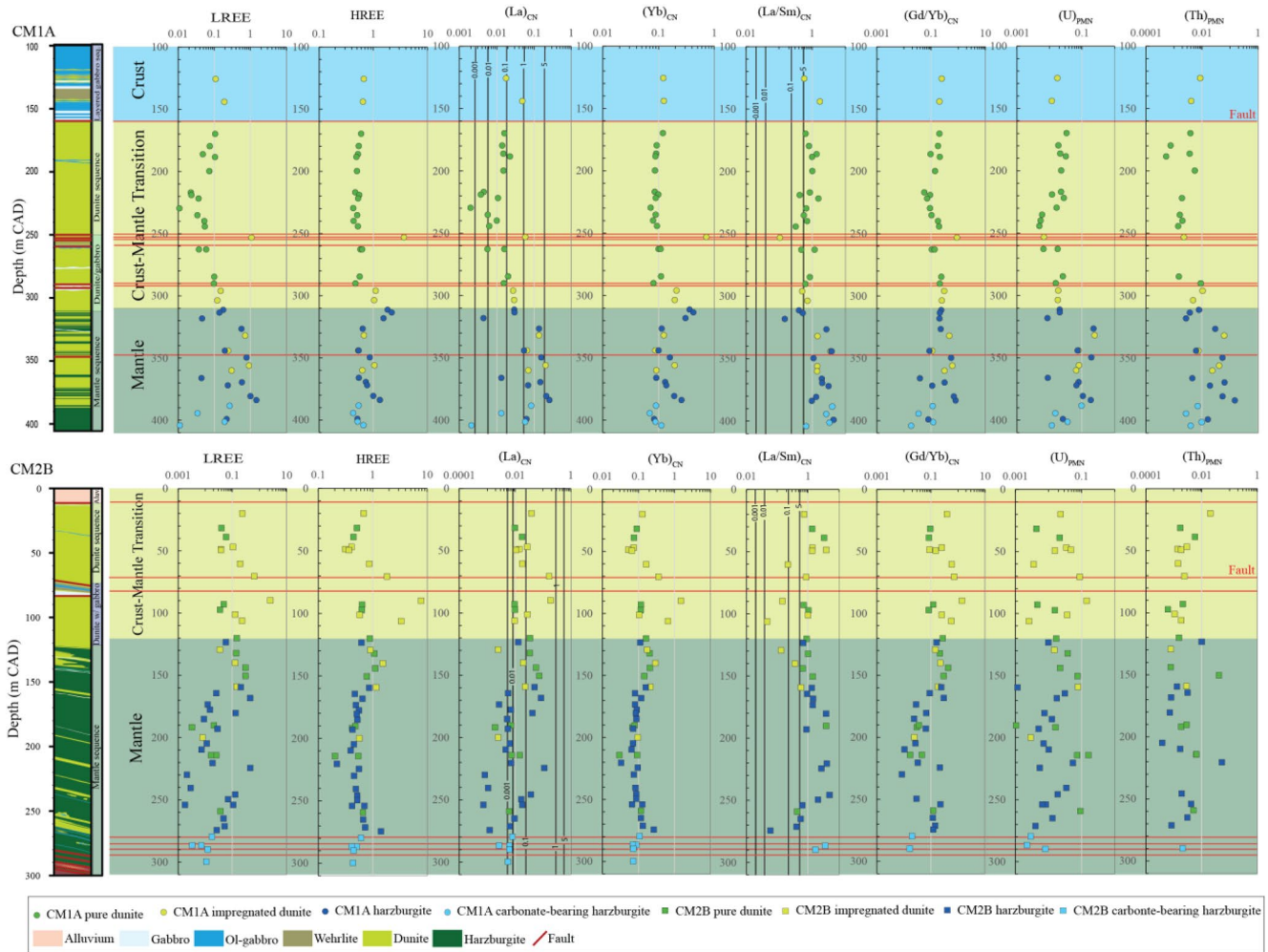


Figure 6. Downhole plots of (from left to right) (LREE ($\text{La} + \text{Ce} + \text{Pr} + \text{Nd}$)_{CN}) (HREE ($\text{Ho} + \text{Er} + \text{Tm} + \text{Yb} + \text{Lu}$)_{CN}) (La)_{CN} (Yb)_{CN} (La/Sm)_{CN} (Gd/Yb)_{CN} (U)_{PMN} and (Th)_{PMN} in whole rock samples recovered at Hole CM1A and CM2B (CN: chondrite-normalized; PMN: PM-normalized). The thick solid red lines indicate the faults, and the thicker solid black lines indicate the (La)_{CN} and (La/Sm)_{CN} concentrations in the most residual peridotites from “Plate model” of Vernières et al. (1997) applied by Godard et al. (2000) (experiment b and d, see Figure 9), the numbers on the black lines indicate the proportions of trapped melt (in percentage) issued from the models. Normalizing chondrite and Primitive Mantle values are from Barrat et al. (2012) and Sun and McDonough (1989) respectively.

($\text{La}_{\text{CN}}/\text{Sm}_{\text{CN}} = 3.21 \pm 1.18$) and HREE ($\text{Gd}_{\text{CN}}/\text{Yb}_{\text{CN}} = 0.07 \pm 0.06$). Seven samples show a positive Eu anomaly ($(\text{Eu}/\text{Eu}^*)_{\text{CN}} = 3.36 \pm 1.69$).

The mantle pure dunites and impregnated dunites show two types of chondrite-normalized REE patterns: linear REE patterns (3 pure dunites from CM2B and six impregnated dunites (3 from CM1A and 3 from CM2B)) and U- or V-shaped REE patterns (5 pure dunites and one impregnated dunites from CM2B). In detail the linear REE pattern are subdivided to: (a) flat linear REE patterns displayed by the three CM1A impregnated dunites, they are characterized by roughly similar LREE ($\text{La}_{\text{CN}} = 0.14 \pm 0.07$), MREE ($\text{Sm}_{\text{CN}} = 0.10 \pm 0.05$), and HREE ($\text{Yb}_{\text{CN}} = 0.18 \pm 0.05$) concentrations, together with a positive Eu anomaly ($(\text{Eu}/\text{Eu}^*)_{\text{CN}} = 2.06 \pm 0.65$). (b) LREE-depleted linear REE patterns displayed by 3 pure dunites and three impregnated dunites from CM2B show a progressive depletion from HREE ($\text{Gd}_{\text{CN}}/\text{Yb}_{\text{CN}} = 0.25 \pm 0.16$ and 0.18 ± 0.04 , $\text{Yb}_{\text{CN}} = 0.22 \pm 0.05$ and 0.28 ± 0.07 respectively) to MREE ($\text{Sm}_{\text{CN}} = 0.04 \pm 0.03$ and 0.04 ± 0.02 , $\text{Gd}_{\text{CN}} = 0.06 \pm 0.04$ and 0.05 ± 0.02

Figure 5. Whole rock major compositions of samples recovered at Holes CM1A and CM2B compared to other crust-mantle transition dunites and mantle harzburgites/lherzolites from the Oman ophiolite (Gerbert-Gaillard, 2002; Godard et al., 2000; Hanghøj et al., 2010; Khedr et al., 2014; Monnier et al., 2006; Nicolle et al., 2016; Rospabé, Benoit, & Candaudap, 2018; Rospabé, Benoit et al., 2019; Takazawa et al., 2003). (a) MgO/SiO_2 versus $\text{Al}_2\text{O}_3/\text{SiO}_2$, (b) total iron as FeO versus MgO , and (c) Al_2O_3 versus CaO . Compositions are recalculated on a volatile-free basis. Red bar in panel (a) represents the silicate Earth differentiation trend (or “terrestrial array”) (Jagoutz et al., 1979). Dashed gray lines in panels (b) and (c) represent constant $\text{Mg}\#$ and $\text{Al}_2\text{O}_3/\text{CaO}$ ratios respectively.

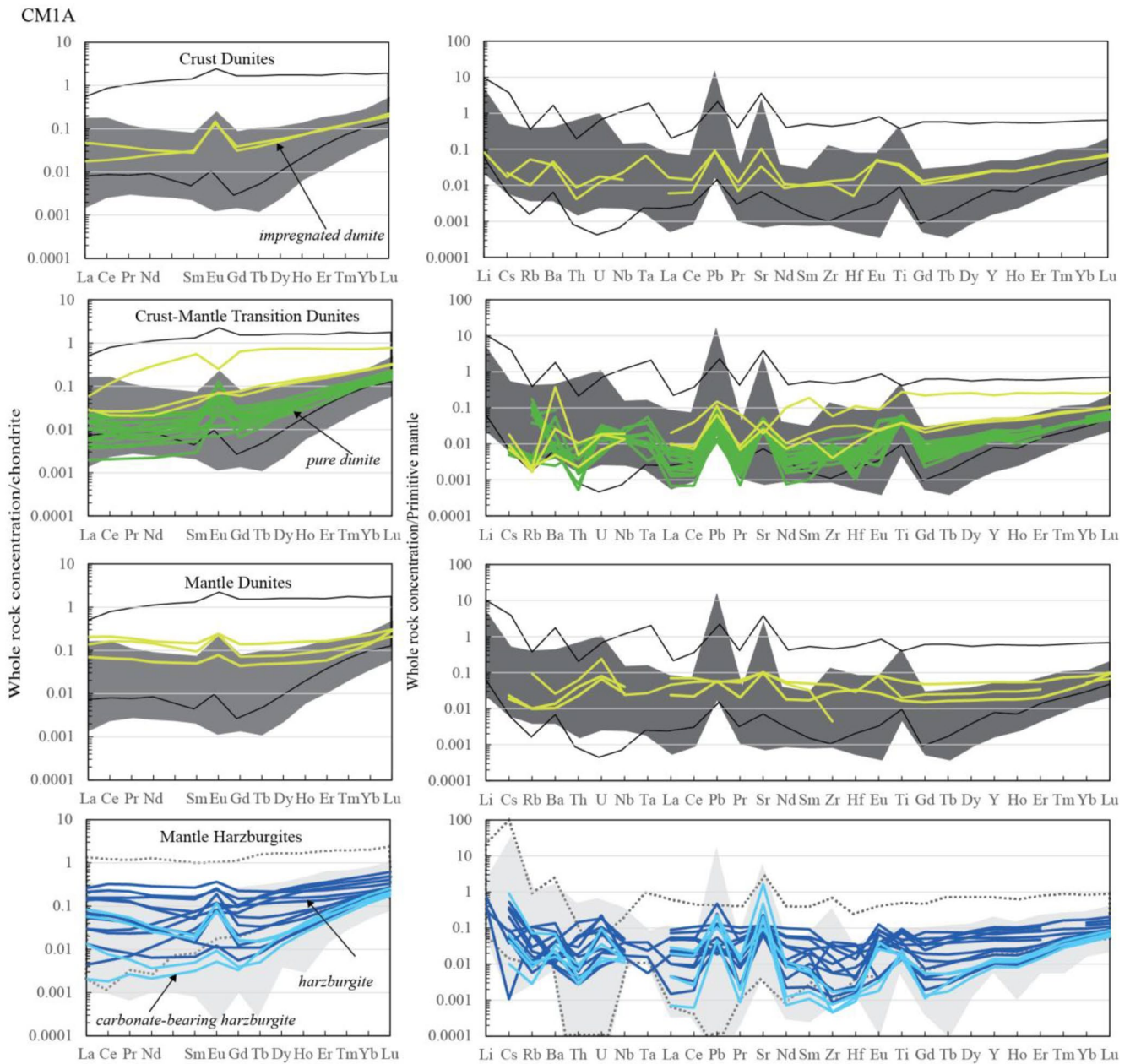


Figure 7a. Chondrite-normalized REE and Primitive Mantle (PM)-normalized multi-element patterns of pure dunites, impregnated dunites, harzburgites and carbonate-bearing harzburgites from the crust, crust-mantle transition zone and mantle sections recovered at Hole CM1A. Other pure dunites (dark gray field formed) and impregnated dunites (field formed by black line) from the crust-mantle transition, and harzburgites (light gray field) and lherzolites (field formed by dashed line) patterns from the mantle section of the whole Oman ophiolite are reported for comparison (Gerbert-Gaillard, 2002; Girardeau et al., 2002; Godard et al., 2000; Hanghøj et al., 2010; Khedr et al., 2014; Lippard et al., 1986; Monnier et al., 2006; Nicolle et al., 2016; Rospabé, Benoit, & Candaudap, 2018; Rospabé, Benoit et al., 2019; Takazawa et al., 2003). Normalizing chondrite and PM values are from Barrat et al. (2012) and Sun and McDonough (1989) respectively.

respectively) to LREE ($La_{CN}/Sm_{CN} = 0.71 \pm 0.28$ and 0.37 ± 0.23 , $La_{CN} = 0.03 \pm 0.02$ and 0.02 ± 0.01 respectively), 1 sample shows a positive Eu anomaly ($(Eu/Eu^*)_{CN} = 1.60$). The U- or V-shaped REE patterns (5 pure dunites and one impregnated dunites from CM2B) are characterized by significant MREE depletion relative to LREE ($La_{CN}/Sm_{CN} = 2.66 \pm 1.76$) and HREE ($Gd_{CN}/Yb_{CN} = 0.08 \pm 0.12$), 2 pure dunites display a positive Eu anomaly ($(Eu/Eu^*)_{CN} = 2.91$ and 2.54).

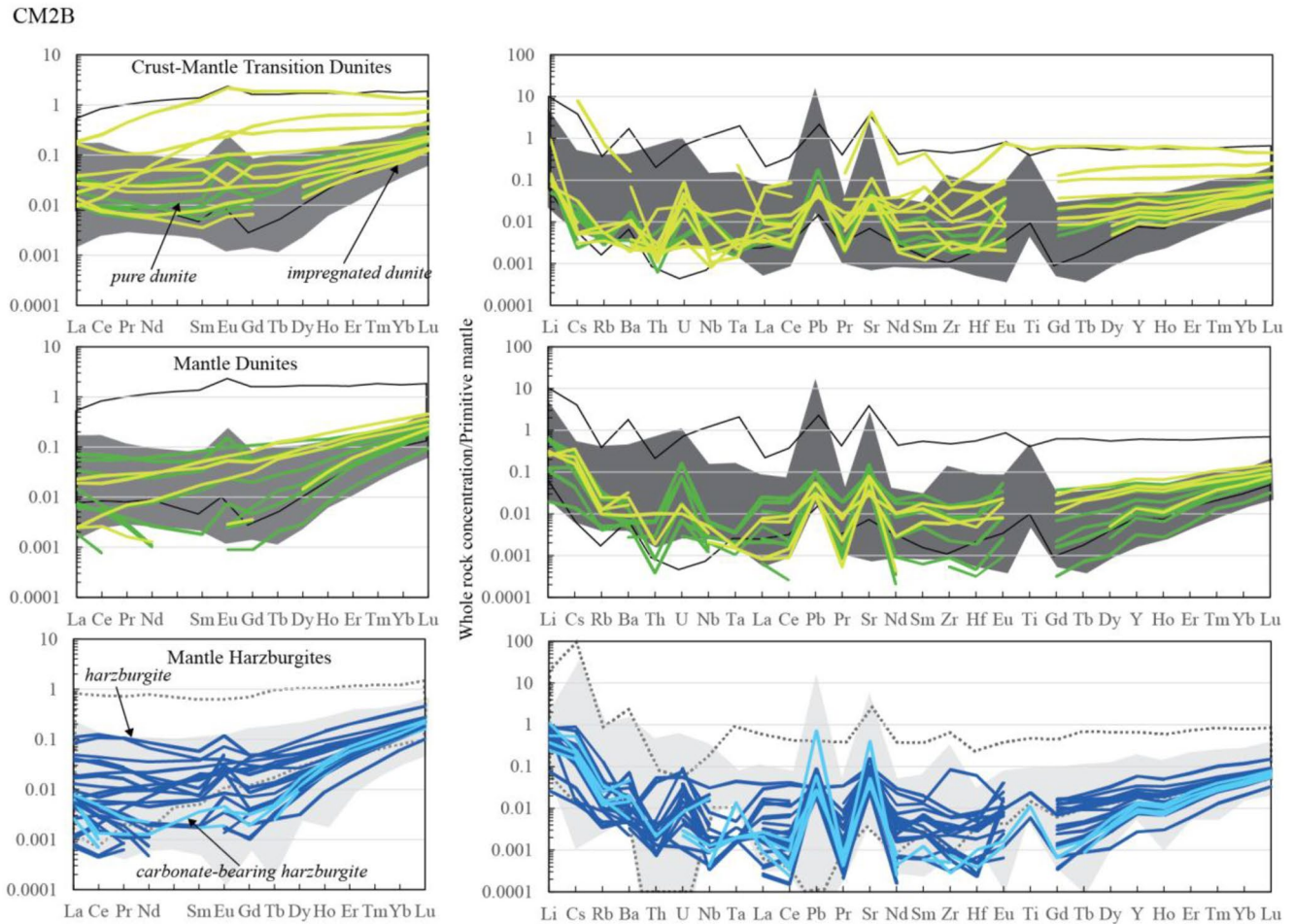


Figure 7b. Chondrite-normalized REE and Primitive Mantle (PM)-normalized multi-element patterns of pure dunites, impregnated dunites, harzburgites and carbonate-bearing harzburgites from the crust-mantle transition zone and mantle sections recovered at Hole CM2B. Other pure dunites (dark gray field formed) and impregnated dunites (field formed by black line) from the crust-mantle transition, and harzburgites (light gray field) and lherzolites (field formed by dashed line) patterns from the mantle section of the whole Oman ophiolite are reported for comparison (Gerbert-Gaillard, 2002; Girardeau et al., 2002; Godard et al., 2000; Hanghøj et al., 2010; Khedr et al., 2014; Lippard et al., 1986; Monnier et al., 2006; Nicolle et al., 2016; Rospabé, Benoit, & Candaudap, 2018; Rospabé, Benoit et al., 2019; Takazawa et al., 2003). Normalizing chondrite and PM values are from Barrat et al. (2012) and Sun and McDonough (1989) respectively.

3.4.2. The Crustal-Mantle Transition Zone Sequence (CMTZ)

The pure dunites from the CMTZ show two types of chondrite-normalized REE patterns: (a) U-shaped REE pattern displayed by 11 pure dunites (6 from CM1A and 5 from CM2B), with MREE depletion relative to LREE ($La_{CN}/Sm_{CN} < 3.34$) and HREE ($Gd_{CN}/Yb_{CN} < 0.27$). Some samples also have positive Eu anomalies (4 samples from CM1A and 3 samples from CM2B ($Eu/Eu^*_{CN} = 3.62 \pm 2.49$)). (b) Linear LREE-depleted or slightly concave-upward REE patterns displayed by 10 pure dunites from Hole CM1A ($La_{CN}/Yb_{CN} = 0.07 \pm 0.05$) with similar HREE concentrations ($Yb_{CN} = 0.13 \pm 0.02$) and lower LREE and MREE variation compared to HREE ($La_{CN} = 0.01 \pm 0.01$; $Gd_{CN} = 0.02 \pm 0.01$). Most samples display a positive Eu anomaly (6 samples ($Eu/Eu^*_{CN} = 4.43 \pm 2.44$)).

The CMTZ impregnated dunites display three types of chondrite-normalized REE patterns: (a) The linear REE patterns displayed by five impregnated dunites (2 from CM1A and 3 from CM2B) are characterized by a progressive depletion from HREE ($Gd_{CN}/Yb_{CN} = 0.38 \pm 0.20$, $Yb_{CN} = 0.23 \pm 0.09$) to MREE ($Sm_{CN} = 0.07 \pm 0.06$ and $Gd_{CN} = 0.10 \pm 0.09$) to LREE ($La_{CN}/Sm_{CN} = 0.77 \pm 0.19$, $La_{CN} = 0.05 \pm 0.06$), 2 samples show a positive and negative Eu anomaly ($Eu/Eu^*_{CN} = 2.23$ and 0.45 respectively). (b) 3 samples from CM2B display U-shaped REE pattern, with MREE depletion relative to LREE ($La_{CN}/Sm_{CN} < 3.93$) and HREE ($0.09 < Gd_{CN}/Yb_{CN} < 0.25$). (c) One sample from CM1A and three samples from CM2B display concave-upward patterns

characterized by a nearly flat slope of the HREE segment ($Gd_{CN}/Yb_{CN} = 0.86 \pm 0.39$) followed by a progressive depletion from MREE to LREE ($La_{CN}/Sm_{CN} = 0.13 \pm 0.07$). One CM1A impregnated dunite shows a negative Eu anomaly ($(Eu/Eu^*)_{CN} = 0.42$).

3.4.3. The Crustal Sequence (CS)

The two impregnated dunites from the Hole CM1A CS (C5707 A-51Z-1 W, 31–39.0 cm, 125.60 m depth, and C5707 A-58Z-2 W, 1.0–6.0 cm, 143.94 m depth) display relatively linear (REE) patterns characterized by a steady decrease of REE abundances HREE to LREE, as well as by a clear positive Eu anomaly ($(Eu/Eu^*)_{CN} = 3.8–5.0$).

The PM-normalized multi-element patterns of most harzburgites and carb-bearing harzburgites exhibit strong to moderate enrichments in LILE, Th, U, Nb and Ta relative to LREE (e.g., averaged $Rb_{PMN}/La_{PMN} = 12.95$ and 18.24 ; $U_{PMN}/La_{PMN} = 4.64$ and 4.45 ; $Nb_{PMN}/La_{PMN} = 2.02$ and 4.30 respectively). The carb-bearing harzburgites display stronger Pb, Sr and Ti positive anomalies (averaged $Pb_{PMN}/Ce_{PMN} = 145.23$; $Sr_{PMN}/Nd_{PMN} = 373.50$; $Ti_{PMN}/Gd_{PMN} = 11.09$) compared to the harzburgite (averaged $Pb_{PMN}/Ce_{PMN} = 25.83$; $Sr_{PMN}/Nd_{PMN} = 30.21$; $Ti_{PMN}/Gd_{PMN} = 3.52$). Most pure dunites show similar enrichments exhibited by the harzburgites and carb-bearing harzburgites in LILE, Th, U, Nb and Ta relative to LREE (e.g., averaged $Rb_{PMN}/La_{PMN} = 20.0$; $U_{PMN}/La_{PMN} = 5.12$; $Nb_{PMN}/La_{PMN} = 4.10$), but with smaller Pb and Sr positive anomalies (averaged $Pb_{PMN}/Ce_{PMN} = 19.68$; $Sr_{PMN}/Nd_{PMN} = 29.05$). The pure dunites display stronger Ti positive anomalies compared to the harzburgites and smaller compared to the carb-bearing harzburgites ($Ti_{PMN}/Gd_{PMN} = 8.98$). The impregnated dunites exhibit moderate LILE, Th, U, Nb and Ta enrichments relative to LREE (e.g., averaged $Rb_{PMN}/La_{PMN} = 3.94$; $U_{PMN}/La_{PMN} = 3.12$; $Nb_{PMN}/La_{PMN} = 1.05$), and the smallest Pb, Sr and Ti positive anomalies compared to all groups of rocks (averaged $Pb_{PMN}/Ce_{PMN} = 9.99$; $Sr_{PMN}/Nd_{PMN} = 14.03$; $Ti_{PMN}/Gd_{PMN} = 1.62$).

4. Discussion

Most studies of the ultramafic rocks from the Oman ophiolite consider the dunites to be channels in the mantle or massive at the crust-mantle transition, and replacive in origin. In this model, the dunites represent residues of reaction between a melt undersaturated in silica at low pressure and the host mantle harzburgites during a melt percolation event that led to the complete consumption of opx and to the concomitant precipitation of ol (e.g., Abily & Ceuleneer, 2013; Boudier & Nicolas, 1995; Braun & Kelemen, 2002; Godard et al., 2000; Kelemen et al., 1995, 1997; Koga et al., 2001; Rabinowicz et al., 1987; Rospabé et al., 2017; Rospabé, Benoit, & Candaudap, 2018; Rospabé, Benoit, et al., 2019). The hypothesis of the replacive origin of the dunites, also proposed for other ophiolitic sections and for dunites associated with abyssal peridotites (e.g., Dick & Natland, 1996; Kelemen, 1990; Godard et al., 2008; Quick, 1981b, 1981a), contrasts with an older cumulative model, in which ol crystallization and accumulation created the lowermost part of the oceanic crust (e.g., Elthon, 1979; O'Hara, 1965; Smewing, 1981). Alternatively, it has been proposed that the crust-mantle transition of the Oman ophiolite may be of double origin, with the lower 80% as replacive and the upper 20% as cumulates (Abily & Ceuleneer, 2013). In the case of the OmanDP CM cores, the alternations between dunites and mantle harzburgites at the top of the mantle sequence is consistent with a melt/rock reaction origin, a feature observed at crust-mantle transitions of many massifs along the Oman ophiolite (e.g., Boudier & Nicolas, 1995) and that cannot be accounted for by a simple fractional crystallization process.

Structural and petrological mappings of the Oman ophiolite have revealed contrasting domains along the ophiolite. Especially, the spatially varying nature and composition of the dikes cross-cutting the mantle section reflect formation involving a MORB-like melt mainly in the south-eastern Nakhil, Samail and Wadi Tayin massifs (troctolite and ol-gabbro dikes), contrasting with a more widespread depleted, calc-alkaline magma composition elsewhere (mostly gabbro and pyroxenite dikes; Python & Ceuleneer, 2003; Python et al., 2008). The MOR-like area characterizes a NW-SE oriented paleo-spreading segment that seems to have developed within older, already accreted lithosphere of depleted calc-alkaline affinity (Ceuleneer et al., 1988, 1996; Gerbert-Gaillard, 2002; Godard et al., 2000; Nicolas et al., 2000; Python & Ceuleneer, 2003). This MORB segment is hypothesized to have been centered on, and fed with melts by, the fossil mantle diapir of the Maqсад area in the Samail massif (Ceuleneer et al., 1988; Jousset et al., 1998; Rabinowicz et al., 1987). According to the published structural and petrological maps, the drilling site is located within the area where melts were MORB-like, near the NE limit of the paleo spreading segment. This delimitation has been defined as the Makhbiyah shear zone in the Wadi Tayin

massif, making the contact with the older lithosphere (Nicolas & Boudier, 2008). Accordingly, it is reasonable to consider that a MORB-like melt played an important role in the formation of the CM dunites and harzburgites.

4.1. Effects of Serpentinization and Carbonation on the Composition of Dunites and Harzburgites

In some cases, alteration, especially serpentinization of ultramafic rocks (sometimes associated with mineralization related to hydrothermal activity), may significantly modify bulk-rock chemical composition (e.g., Beinlich et al., 2020; de Obeso & Kelemen, 2018; Gruau et al., 1998; Hodel et al., 2018; Malvoisin, 2015; Paulick et al., 2006; Snow & Dick, 1995). As described above, the dunites and harzburgites from the crust-mantle transition and mantle section of Holes CM1A and CM2B are extensively serpentinized (Figure 2), up to 100% in many samples. In addition, strong carb-veining affected parts of the cores, especially at the base of Hole CM2B where it is intensely faulted (carb-bearing harzburgites, Figure 3, CO₂ and CaCO₃ logs). To decipher the effects of such significant fluid/rock interactions on the composition of OmanDP CM samples is critical (especially on the trace elements). It particularly concerns the dunites, because of their more altered character (perhaps related to higher ol mode), and because their trace element budget was more significantly controlled by primary ol and trace phases such as pyroxenes before alteration (unlike the harzburgites that contain abundant residual pyroxenes).

The LOI content is generally higher in carb-bearing harzburgite (averaged LOI = 13.04 ± 9.57 wt.%), pure dunites (averaged LOI = 13.92 ± 1.21 wt.%) and impregnated dunites (averaged LOI = 13.33 ± 2.02 wt.%) than in harzburgites (averaged LOI = 11.91 ± 1.53 wt.%). Serpentinization of many of the studied samples appears to have led to enrichment in SiO₂ as already observed in abyssal peridotites affected by a Si addition, and/or magnesium loss (e.g., de Obeso & Kelemen, 2018; Paulick et al., 2006; Snow & Dick, 1995). This open system behavior is confirmed by the plot of some dunites (3 from CM2B) and impregnated dunites (4 from CM1A and 4 from CM2B) below the mantle fractionation array at the same field as the harzburgites and the carb-bearing harzburgites (Figure 5a), suggesting MgO loss and/or SiO₂ enrichment as reported in pervasively serpentinized abyssal peridotites or talc-bearing serpentinites (de Obeso & Kelemen, 2018; Paulick et al., 2006; Snow & Dick, 1995). This may be the reason why there are elevated normative pyroxene modes in samples that were classified as dunites based on macroscopic (hand specimen) and microscopic (thin sections) observations (Figure SD-1 in Supporting Information S1, Table S1). Some of these dunites have no pyroxenes or pyroxene pseudomorphs in thin section. This is supported by XRD analyses performed during ChikyuOman 2018 Phase two Leg 3 which revealed the widespread occurrence of brc associated with other alteration minerals (Kelemen et al., 2020a, 2020b). It also appears clear that the higher CaCO₃ (averaged CaCO₃ = 3.93 ± 10.85 wt.% compared to 0.40 ± 0.54 wt.% in harzburgites) together with higher CO₂ contents (averaged CO₂ = 2.82 ± 9.501 wt.% compared to 0.20 ± 0.25 wt.% in harzburgites) in the carb-bearing harzburgites at the base of CM1A and CM2B (4 from CM1A and 4 from CM2B) are related to carb-veins. However, the covariation of Ni and Co contents with the XMg suggests that the possible precipitation of sulfides (Kelemen et al., 2020a, 2020b) related to these strong water/rock interactions did not erase the primary compositions in these elements.

The plots of the concentration of several trace elements as a function of the LOI (Figures 8a–8c) and of the CO₂ and CaCO₃ contents show no clear correlation. On the contrary, some reasonably good covariations are observed between Th and U, Nb and especially La on one hand (Figures 8h–8j), and Yb, Ti and Hf on the other hand (Figures 8n–8o); the Zr content is partially correlated with both Th and Yb (Figures 8f–8k). Since Th and Ti are generally considered immobile during alteration processes (e.g., Kogiso et al., 1997; Niu, 2004; Paulick et al., 2006), these trends probably reflect one or more overlapping geochemical signatures acquired during high temperature, magmatic processes rather than during a later serpentinization event. The large ion lithophile elements as well as Li and Pb do not correlate with the LOI nor with other elements (Figures 8b–8g, 8l, 8m), and their compositions may result from the overprint of several processes having operated over a large range of temperatures and conditions, from igneous to alteration events. Accordingly, only the concentrations in REE, HFSE and Th-U, will be used to discuss the igneous processes that led to the formation of the dunites from the CMTZ and mantle sequence sampled by the CM Holes.

4.2. Partial Melting Versus Melt-Rock Reaction in the Oman Ophiolite Mantle Section

The mantle section of CM Holes (Wadi Tayin massif) is composed of refractory harzburgites with relatively homogeneous modal and major element compositions (excluding some major elements e.g., CaO and Na₂O,

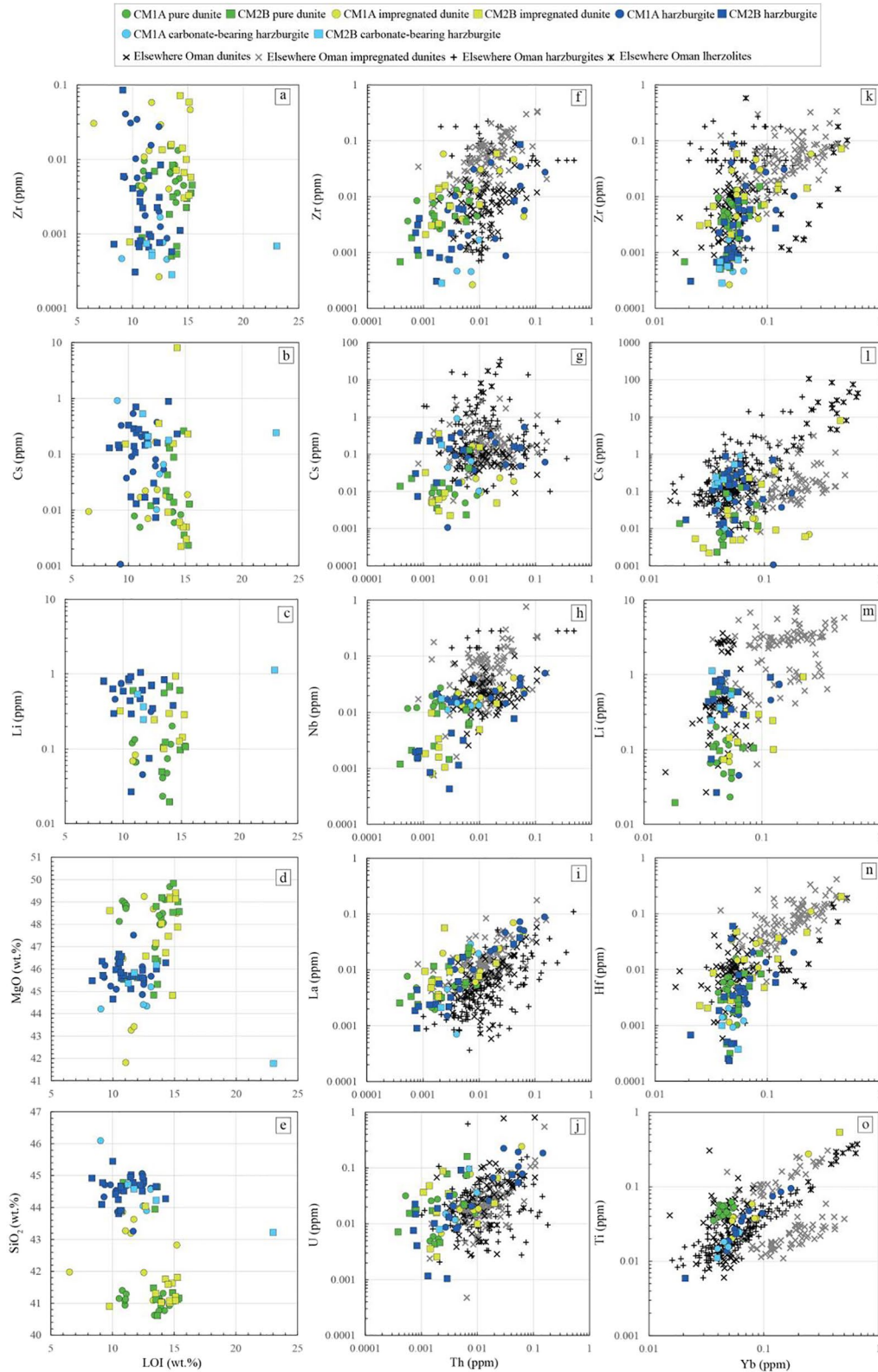


Figure 8.

Figures 4 and 5) and more variable trace element contents (Figures 6, 7a, and 7b). Significant geochemical variability of the mantle peridotites has also been observed all along the Oman ophiolite. In some cases, previous geochemical studies inferred the overprint of partial melting and melt/peridotite reaction processes in the mantle harzburgite signatures (e.g., Gerbert-Gaillard, 2002; Girardeau et al., 2002; Godard et al., 2000; Hanghøj et al., 2010; Kanke & Takazawa, 2014; Khedr et al., 2014; Le Mée et al., 2004; Monnier et al., 2006; Takazawa et al., 2003). Two different geochemical trends are combined in the trace element contents of all samples studied here. On one hand, Yb shows a good correlation with Ti and some HFSE (Figure 8o). HREE have been demonstrated to be less impacted than MREE and especially LREE during melt-peridotite reactions such as melt/rock re-equilibration during melt migration or in response to conversion of harzburgite to dunite (e.g., Godard et al., 1995; Kelemen, 1990; Navon & Stolper, 1987; Prinzhofer & Allègre, 1985; Spiegelman & Kelemen, 2003; Vernières et al., 1997; Rospabé, Benoit, & Candaudap, 2018). Therefore, these correlations may have been formed during partial melting, with little or no overprint by subsequent melt-peridotite interactions at shallow depth. On the other hand, we observe a good correlation between Th, U and La, and partially with the HFSE (e.g., Nb, Figures 8h–8j), that does not correlate with Yb or Ti concentrations. As the U-/V-shape of the REE patterns, resulting from the selective enrichment in LREE relative to MREE and HREE in peridotites, may be attributed to chromatographic fractionation associated with interstitial melt percolation and/or to the transformation of harzburgite into dunite (e.g., Godard et al., 1995; Navon & Stolper, 1987; Prinzhofer & Allègre, 1985; Rospabé, Benoit, & Candaudap, 2018; Vernières et al., 1997), we interpret this second geochemical signature as the overprint of melt-peridotite reaction processes.

4.2.1. Geochemical Logs

Vertical chemical trends are observed along CM Holes, especially in REE (e.g., La, Yb; Figure 6), and in some major elements (e.g., FeO, MgO, CaO, Na₂O; Figure 4). These chemical trends are continuous over tens of meters, and alternate between increasing and decreasing (“zigzag” patterns) with a characteristic thickness of ~50 m. Abrupt changes in these trends, particularly in Yb, LREE and HREE concentrations, are mostly associated with the presence of faults (Figure 6). The trends observed in CM1A and CM2B dunites and harzburgites do not show any significant correlation as a function of LOI, CO₂, or CaCO₃ contents (Figures 3 and 8). This, together with the continuity of each individual trend, suggests that the trends were imprinted at high temperature and are not related to post-magmatic, low temperature events. Furthermore, the trends are observed in both dunites and harzburgites in the mantle section, independent of dunite and harzburgite alternations. Similar trend changes attributed to the focus of the percolation/migration of melts or HT fluids along faults have been observed for the Maqsad CMTZ dunites, with the same characteristic thickness of about 50 m (Rospabé, Benoit et al., 2019; Rospabé, Ceuleneer et al., 2020). Our results seem to confirm the significant impact of deep-seated syn-magmatic faults on the development of the crust-mantle transition at the expense of the shallower mantle and the recorded whole rock chemical signatures, in addition to their impact on the formation of the lower oceanic crust (Abily et al., 2021; see also, 2011; Sauter et al., 2021). Such structural characters must have developed early and are not just restricted to the Maqsad area (e.g., Rospabé (2018) and Abily et al. (2021) for other Oman areas and Sauter et al. (2021) for present-day oceans).

4.2.2. The Origin of the Harzburgite REE Pattern Shapes and Cryptic and Modal Mantle Refertilization in Oman Ophiolite

CM mantle harzburgites display two types of chondrite-normalized REE patterns: (a) linear to flat linear REE patterns characterized by a progressive depletion from HREE to MREE to LREE, some samples show similar LREE and HREE concentrations and slightly lower LREE and MREE variation compared to HREE; (b) U- or V-shaped REE patterns reflecting significant MREE depletion relative to LREE and HREE. CM harzburgites are enriched in LREE relative to MREE with 12 harzburgites that are depleted in LREE relative to MREE and HREE; this is not expected for mantle residues after near-fractional partial melting (Godard et al., 1995, 2000, 2008; Gruau et al., 1998; Johnson & Dick, 1992; Johnson et al., 1990; Kelemen et al., 1997; Navon & Stolper, 1987; Prinzhofer & Allègre, 1985; Vernières et al., 1997). The linear REE patterns observed in CM harzburgites are

Figure 8. Plots of LOI (wt.%) versus Zr (ppm), Cs (ppm), Li (ppm), MgO (wt.%), and SiO₂ (wt.%); Th (ppm) versus Zr (ppm), Cs (ppm), Nb (ppm), La (ppm), and U (ppm); Yb (ppm) versus Zr (ppm), Cs (ppm), Li (ppm), Hf (ppm), and Ti (ppm) in dunite and harzburgites recovered at Hole CM1A and CM2B. Other pure dunites, impregnated dunites, harzburgites and lherzolites compositions from the crust-mantle and the mantle section of the whole Oman ophiolite are reported for comparison (Gerbert-Gaillard, 2002; Girardeau et al., 2002; Godard et al., 2000; Hanghøj et al., 2010; Khedr et al., 2014; Lippard et al., 1986; Monnier et al., 2006; Nicolle et al., 2016; Rospabé, Benoit, & Candaudap, 2018; Rospabé, Benoit et al., 2019; Takazawa et al., 2003).

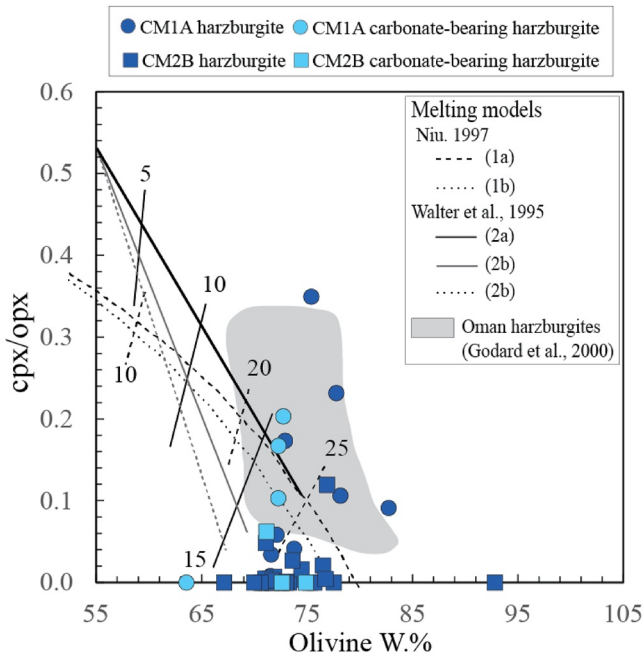


Figure 9. Modal compositions of the analyzed CM harzburgites plotted on a cpx/opx versus olivine (ol) diagram. The field defined by the mantle harzburgites studied in Godard et al., 2000 is reported for comparison. Published melting models are also shown for comparison: model 1 represents the polybaric melting model after Niu (1997) (1a) with and (1b) without excess ol; model 2 represents the isobaric melting after Walter et al. (1995) at 11 (2a), 16 (2b) and 17 kbar (2c). The initial modal composition is given by Niu (1997) for polybaric melting and was fixed for isobaric melting as: 55% ol, 28% opx, 15% cpx and 2% sp. Numbers refer to percent melting degrees.

similar to the main harzburgites mantle section REE patterns from Wadi Tayin described by Godard et al. (2000); these harzburgites have relatively homogeneous modal and major element compositions. The Maqsad diapir harzburgites and Samail massif *cpx*-harzburgites display concave-upward and “spoon-shaped” REE patterns respectively, these patterns are not observed in CM Wadi Tayin harzburgites. The Maqsad diapir has been interpreted as frozen upwelling mantle that fed a former spreading center (Ceuleener et al., 1988). The concave-upward REE patterns and the higher $\text{Al}_2\text{O}_3/\text{CaO}$ ratios and TiO_2 contents in the diapir harzburgites result from the feedback between deformation and melt percolation, and the *cpx*-harzburgites REE patterns and chemical characteristics are interpreted as a result of a *cpx* forming melt-rock reaction at decreasing melt mass (at near-solidus conditions) along the lithosphere-asthenosphere boundary (Godard et al., 2000).

Figure 9 shows the modal composition of CM1A, CM2B (harzburgites and carb-bearing harzburgites) and Nakhl-Samail-Wadi Tayin massif samples (harzburgites, Godard et al., 2000) plotted with two published melting models: model 1 represents the Niu (1997) polybaric melting model (1a) with and (1b) without excess ol; model 2 represents the Walter et al. (1995) isobaric melting at 11 (2a), 16 (2b) and 17 kbar (2c). The figure indicates that CM harzburgites could result from high degrees of partial melting and melt extraction in the range of 15%–30% (e.g., Asimow et al., 2001; Kelemen, 1990; Kelemen et al., 1995, 1992; Niu, 1997; Walter et al., 1995), as suggested by Godard et al. (2000) for the main harzburgite section of the MORB-like, NW-SE paleo spreading segment (Nakhl-Samail-Wadi Tayin massifs). This range is higher than melting degrees producing MORB in present-day oceans (5%–10%; Langmuir et al., 1992) and high-Ti magmas such as those forming the sheeted dyke complex and the MORB-like lava sequence in Oman (Godard et al., 2006; Lippard et al., 1986). However, Niu (1997) and Dick and Natland (1996) have reconciled this inconsistency by considering that abyssal peridotites represent only the shallowest part of the mantle column affected by partial melting and therefore record the highest melting degrees. In contrast, MORB are thought to represent integrated, mixed melt fractions from polybaric decompression melting over 60–100 km at ascent melting column and therefore record average melting degrees.

The linear REE patterns of some studied harzburgites do not show features of strong LREE depletion, but most of the other CM harzburgites show U-shaped REE patterns, characterized by LREE enrichment. This, together with the high (primary) proportion of ol (75%–90%) observed in some samples, point to the fact that near fractional partial melting alone fails to explain the harzburgite geochemical signatures along the CM cores. Vernières et al. (1997) noted that the relatively unfractionated REE distribution may simply result from melt transport through the melting peridotites, as an “open-system melting process”. This process would result in a negative correlation between LREE/HREE ratios and peridotite fertility, as commonly observed in other ophiolites (e.g., Prinzhofer & Allègre, 1985). It results from the competition between the partial melting continuously depleting the mantle residue on one hand and chromatographic effects related to the melt extraction that enrich the residue in the most incompatible elements on the other hand (e.g., Johnson et al., 1990; Navon & Stolper, 1987; Niu, 2004; Spiegelman & Kelemen, 2003; Takazawa et al., 1992).

CM harzburgites show good correlations among Yb, Ti and Hf concentrations, indicating that the variability in HREE was more likely controlled by the melting process rather than by the overprint of melt-rock reaction processes (Figures 8n–8o). We compared the linear REE patterns in CM harzburgites to Vernières et al. (1997) plate model calculations performed by Godard et al. (2000), who modeled trace elements in peridotites from the Nakhl-Samail-Wadi Tayin massifs to explore whether the REE variations observed in the studied harzburgites resulted from reactive porous flow at increasing melt mass, or from partial melting coupled with melt transport (Figure 10). The authors first simulated a standard incremental melting model (experiment a, Figures 10a and Johnson et al., 1990). Then, they simulated reactive porous flow at increasing melt mass in a second model

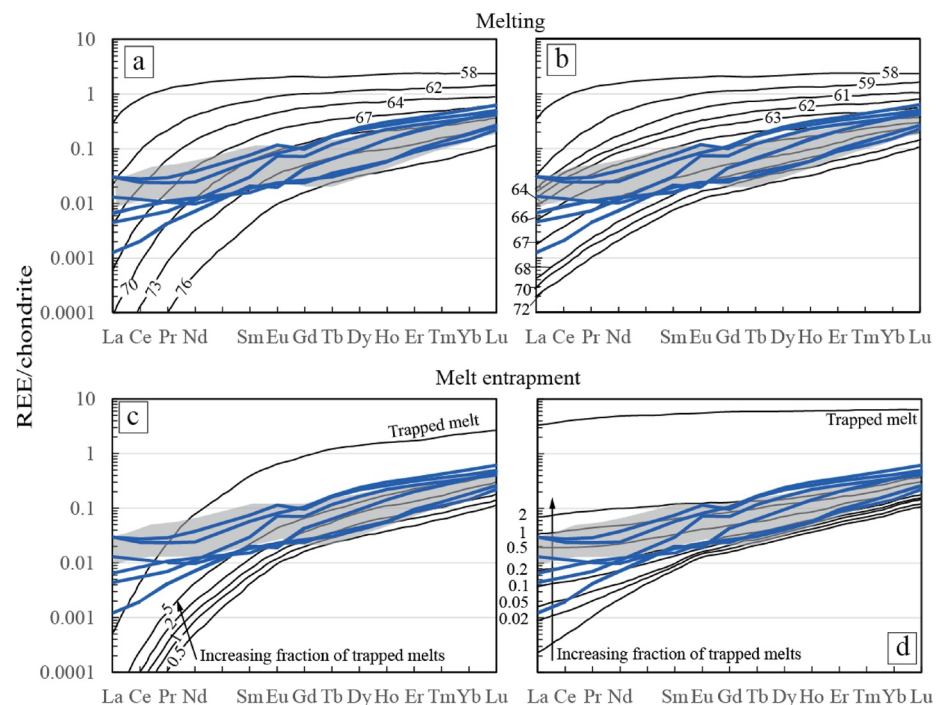


Figure 10. CM1A and CM2B REE linear flat shaped REE patterns (Thicker blue lines) compared to the “Plate model” of Vernières et al. (1997) applied by Godard et al. (2000) to simulate REE variations in a peridotite affected by partial melting with (a) or without (b) melt infiltration. The chondrite-normalized REE patterns of the Oman harzburgites from Godard et al. (2000) (the gray fields, main harzburgite section) are also shown for comparison. The authors simulate standard incremental melting in model (a) and the percolation of fixed N-MORB melt through molten peridotites in model (b). The peridotite initial modal composition was (spinel free): 57% ol, 28% opx and 15% cpx. The melting reaction was taken from Walter et al. (1995). Mineral/melt partition coefficients are the same as those selected by Bedini and Bodinier (1999). Numbers on the chondrite-normalized REE patterns indicate olivine (ol) proportion (in percentage) in residual peridotites. Thicker black lines indicate the REE patterns of the less residual peridotites. In model (a), the most residual peridotite (76% ol) is produced after 21.1% melt extraction. In model (b), the ratio of infiltrated melt to peridotite varies from 0.02 to 0.19 (bottom). Modifications of the REE patterns of residual peridotites due to the presence of equilibrium, trapped melt. Models (c) and (d) show the effect of trapped melt on the most residual peridotites of models (a) and (b), respectively (thicker solid lines). Numbers on the REE patterns indicate the proportions of trapped melt (in percentage). Normalizing chondrite values are from Barrat et al. (2012).

(experiment b, Figure 10b). Experiment (a) produces strongly LREE-depleted peridotite residues, quite different in shape from CM and other Oman harzburgites. This experiment does not provide a better fit to the data when the presence of the trapped melt in the residue is included (Figure 10c). Experiment (b) produces peridotite residues moderately depleted in LREE and with a small amount of trapped melt (0.5%–1%; Figure 10d). The linear REE patterns of harzburgites from Holes CM1A and CM2B are similar to Nakhil-Samail-Wadi Tayin harzburgites of Godard et al. (2000) and well reproduced by experiment (b). The model suggests that part of the studied harzburgites were pervasively percolated by diffuse melt flow which affected their geochemical signature. However, the presence of many dunite intervals at the top of the mantle section requires an opx-consuming reaction between the residual peridotites and infiltrated melts.

The CMTZ pure dunites from CM holes (Wadi Tayin massif) display two types of chondrite-normalized REE patterns: (a) U-shaped REE patterns; (b) Linear LREE-depleted or slightly concave-upward REE patterns with similar HREE, MREE and LREE concentrations, with slightly lower LREE and MREE concentrations compared to HREE in some samples. The CMTZ impregnated dunites display three types of chondrite-normalized REE patterns: (a) linear REE patterns; (b) U-shaped REE patterns; (c) concave-upward patterns characterized by a nearly flat slope of the HREE segment followed by a progressive depletion from MREE to LREE. The Maqsad mantle-crust transition zone pure dunites trace elements are characterized by U-shaped to concave-upward REE patterns (Godard et al., 2000; Rospabé, Benoit, & Candaudap, 2018; Rospabé, Benoit et al., 2019), similar to Maqsad diapir harzburgites (Godard et al., 2000) and to CM mantle dunites and harzburgites trace element

patterns but with larger range of LREE variations in Maqsad MTZ dunites compared to Wadi Tayin CMTZ (CM cores). Maqsad impregnated dunites described by Rospabé, Benoit, & Candaudap, 2018, Rospabé, Benoit et al., 2019 are characterized by similar trace element patterns to CM impregnated dunites, varying between linear LREE-depleted to variably concave-upward trace element patterns. Maqsad MTZ pure and impregnated dunites have been interpreted as end-members that recorded different stage of an initially shared same igneous process (Rospabé, Benoit, & Candaudap, 2018, Rospabé, Benoit et al., 2019). Boudier and Nicolas (1995) and Godard et al. (2000) attest that Maqsad MTZ dunites are diapir harzburgites that were strongly modified by ol-forming melt-rock reactions at high melt/rock ratios. Furthermore, Rospabé, Benoit, & Candaudap. (2018) argue that the pure dunites are residues left after extraction of a percolating melt, whereas the impregnated dunites correspond to a frozen stage before complete melt extraction.

Relatively good covariations are observed in CM dunites and harzburgites between Th and U, Nb and especially La (Figures 8h and 8j), whereas their concentrations are not correlated with the HREE. Following many previous works, we interpret these correlations as the result of melt/peridotite reaction contemporaneously with, and/or subsequent to, the partial melting event discussed above. The CMTZ pure and impregnated dunites from CM Holes display similar REE patterns to the dunites and harzburgites in the mantle section, U-/V-shaped REE patterns (displayed by 11 pure dunites and three impregnated dunites from the CM, CMTZ) cannot be explained by a pure cumulate origin (Figures 7a-7b). Several studies argued that the LREE enrichment relative to MREE cannot be explained by REE partition coefficients between ol and melt (Frey et al., 1978; Hauri & Hart, 1995; Kelemen et al., 1993; Lee et al., 2007; McKenzie & O'Nions, 1991; Sun & Liang, 2014) and may better be explained by peridotite metasomatism as a result of melt-peridotite reactions (e.g., Agranier & Lee, 2007; Godard et al., 1995; Navon & Stolper, 1987; Vernières et al., 1997). Most CM harzburgites display U-shaped REE patterns (15 harzburgites and 8 carb-bearing harzburgites) characterized by a LREE-enrichment compared to the linear REE patterns (12 harzburgites), with strong LREE enrichments indicating extensive interaction with a pervasive melt (Figures 7a-7b; e.g., Gerbert-Gaillard, 2002; Godard et al., 2000; Monnier et al., 2006). CM samples, in particular in Hole CM2B, show downhole variations that indicate a decreasing degree of melting with increasing depth (see Section 4.2.1. Below geochemical logs). Two intervals from 170 to 260 m, and 230–300 m depth, are particularly good examples of this (Figure 6, CM2B e.g., LREE, La, U). The correlations observed between LREE enrichment and an increasing fraction of trapped melt - calculated from experiment (b and d) in the most residual peridotites from “Plate model” of Vernières et al. (1997) applied by Godard et al. (2000) (experiment b and d, see Figure 10) - in CM samples (e.g., La, Figure 6), suggest that CM samples have experienced extensive interaction with a pervasive melt or fluid (for fluid-melt-rock interactions at Maqsad CMTZ see also Rospabé et al., 2017, Rospabé, Benoit, & Candaudap, 2018; Rospabé, Benoit et al., 2019). In the mantle section sampled by the CM cores, crosscutting dunites are widespread and represent end products of the opx-consuming reaction. The harzburgites experienced a more extensive melt flow at a shallow level that contributed to their ol enrichment (Figure 1e, logs). The dunites were probably individualized by channeled percolation at the top of the melting column.

4.3. Petrological and Geochemical Overview of the Mantle-Crust Transition in the SE of the Oman Ophiolite

The CM ultramafic rocks studied in this paper (Wadi Tayin) compared to previously studied Maqsad MTZ dunites and diapir harzburgites show that: (a) the dunites have a replacive origin, they are the products of melt-harzburgite reaction leading to the complete consumption of opx and concomitant precipitation of ol (e.g., Abily & Ceuleneer, 2013; Boudier & Nicolas, 1995; Gerbert-Gaillard, 2002; Godard et al., 2000; Kelemen et al., 1995, 1997; Koga et al., 2001; Rabinowicz et al., 1987; Rospabé, Benoit, & Candaudap, 2018, and references therein). (b) The alternations between dunites and mantle harzburgites observed at the top of the mantle sequence of CM Holes were also observed at the base of the crust-mantle transition in many other massifs along the Oman ophiolite (e.g., Boudier & Nicolas, 1995), recording a snapshot of melt/harzburgite reaction frozen at the time of the uppermost mantle dunitization. (c) The vertical chemical trend changes related to the focus of the percolation/migration along faults observed at CM Holes samples have been previously observed at the Maqsad CMTZ dunites, with the same characteristic thickness of about 50 m (Rospabé, Benoit et al., 2019, Rospabé, Ceuleneer, 2020), confirming the control of synmagmatic faulting on melt/peridotite (\pm fluids) reactions and the petrological and geochemical structuration of the CMTZ.

The two main differences with the crust-mantle transition and mantle section of the neighboring Maqsad area, that have been extensively studied due to their diapir-related features (Ceuleneer et al., 1988), are that (a) if the two sites (Maqsad and OmanDP CM) are both more or less related to the rise of the mantle diapir, the CM site may have had less pronounced magmatic activity due to its distance to the axis of the diapir, and (b) the CM site may have been contaminated by possible remelting of the base of the old lithosphere during the development of the MORB segment, as evidenced in the Sumail massif at the borders of the area influenced by the diapir (Amri et al., 1996; Benoit et al., 1999; Clénet et al., 2010). In cores from Holes CM1A and CM2B, core description revealed the widespread presence of magmatic impregnations in the dunites (i.e., minerals that crystallized interstitially between ol grains during melt migration; e.g., Benn et al., 1988; Dick, 1989), and of magmatic segregation or more intruding dikes (Kelemen et al., 2020a, 2020b). This evidence for melt migration was described within both the crust-mantle transition and the mantle sequence. The impregnations in dunites are composed of pl and clinopyroxene, and the magmatic segregations and dikes are mostly troctolitic and gabbroic, consistent with a MORB-like parent melt produced by decompression melting in the mantle. On the other hand, more exotic websterite and anorthositic gabbros to anorthosites were also observed in the mantle sequence and the dunite/harzburgite alternations.

CM ultramafic rocks studied in this paper (Wadi Tayin) show thus multiple differences compared to the previously studied Maqsad CMTZ dunites and diapir harzburgites: (a) the CM samples have been more intensively affected by low temperature alteration features (serpentinization up to 100% in many samples). (b) The CMTZ is thinner along CM drilled Holes (~150 m, Kelemen et al., 2020a, 2020b) compared to the Maqsad CMTZ (300–400 m, Abily & Ceuleneer, 2013; Boudier & Nicolas, 1995; Jousset & Nicolas, 2000; Rabinowicz et al., 1987; Rospabé, 2018; Rospabé, Benoit et al., 2019). (c) CM pure dunites display lower LREE enrichments compared to the Maqsad ones. (d) Two major trends are observed in the trace element signatures of CM dunites and harzburgites, with good correlations between the Th and U, Nb and LREE on one hand, and between the HREE, Ti and Hf on the other hand, that are not observed at Maqsad. (e) The CM site CMTZ is mostly composed of pure dunites at the top and impregnated dunites at the bottom, whereas the typical structuration of the Maqsad CMTZ is generally composed by impregnated dunites at the top and pure dunites at the bottom (Rospabé, 2018; Rospabé, Benoit et al., 2019). (f) The dunites' impregnation characteristic appears to be different in Maqsad (e.g., mostly pl and clinopyroxene (Abily & Ceuleneer, 2013; Boudier & Nicolas, 1995; Koga et al., 2001) but also widespread opx and amph impregnations in the higher level of the transition zone (Rospabé et al., 2017; Rospabé, Benoit, & Candaudap, et al., 2018; Rospabé, Benoit et al., 2019) compared to CM Hole dunites (pl and clinopyroxene impregnations only). Similarly, exotic silicate inclusions (opx, amph, mica for the more abundant) enclosed in disseminated chromite grains in the dunites from the Maqsad area as well as in associated chromitite ore bodies (Lorand & Ceuleneer, 1989; Leblanc & Ceuleneer, 1991; Schiano et al., 1997; Borisov et al., 2012; Rollinson et al., 2018; Zagrtednov et al., 2018; Rospabé, Ceuleneer et al., 2019, 2020, 2021), suggest the involvement of a fluid or fluid-rich melt in the melt/rock reactions, which were not investigated in existing work on cores CM1A and CM2B - a few chromite schlierens have been sampled along the cores but not studied in details yet. Further investigation of CM ultramafic rock mineral chemistry is need to evaluate these discrepancies between the two CM and Maqsad sites.

All the above similarities and differences between CM Wadi Tayin and Maqsad ultramafic rocks point to a lighter imprint of melt-rock reaction at CM compared to Maqsad (e.g., thinner transition zone, lighter LREE enrichment in dunites, two distinct geochemical trends in trace elements, that perhaps are totally overprinted by stronger melt/rock reaction at Maqsad). This could be the consequence of one or the several factors: It could be related to the structural position of Wadi Tayin (at the periphery of the diapir) and Maqsad (centered on the diapir) leading to different melt/rock ratios (i.e., the geological context), to the timing of the occurrence of the melt-rock interaction, and/or to the nature of the percolating magma/fluid involved in the melt-rock reactions. Further detailed mineral chemistry, trace element geochemical modeling, structural and microstructural studies will be of use for addressing the above questions.

5. Conclusions

Continuous sampling of the Oman CMTZ at Holes CM1A and CM2B, recovered by the OmanDP allows the study of the large range of petrological and geochemical variations in Oman ultramafic rocks with an unprecedented high resolution. Volatile (H₂O and CO₂), and major and trace elements of 56 dunites and 49 harzburgites

from Holes CM1A and CM2B have been analyzed. CM1A and CM2B volatile element contents reflect extensive serpentinization (+/− carbonation) linked to the late-stage interaction with H₂O- and/or CO₂-bearing fluids. The refractory samples are characterized by relatively homogeneous modal and major element compositions, whereas other samples show primary cryptic and modal refertilization. Bulk rock Mg, Si and Al systematics and normative mineral modes suggest that open system behavior during alteration (Mg loss and/or Si gain) affected many samples. However, the trace element concentrations are interpreted as reflecting magmatic processes and exhibit significant variations: the refractory harzburgites characterized by linear REE patterns are interpreted as mantle residues after ≥15% melt extraction. The REE signatures in these samples can be explained by melt transport associated with partial melting. Other harzburgites displaying U-/V-shaped REE patterns are interpreted as the result of interstitial melt percolation. The pure and impregnated dunites from the mantle and the CMTZs are characterized by similar trace element patterns as the mantle harzburgites, they are interpreted as reflecting different stages of ol-forming melt/rock reactions at high melt/rock ratio. The pl and pyroxene minerals present in impregnated dunites indicate that the impregnated dunites represent the stage before complete extraction of the melt from the dunites, whereas the pure dunites represent the melt/rock reaction end-product after complete melt extraction (i.e., compaction of the ol matrix and system closure before/without interstitial pl and clinopyroxene crystallization).

Data Availability Statement

The data set is available on the PANGAEA data archiving platform (<https://doi.org/10.1594/PANGAEA.942402>).

Acknowledgments

This research used samples and/or data provided by the Oman Drilling Project (OmanDP). The OmanDP were funded from the International Continental Scientific Drilling Project (Kelemen, Matter, Teagle Lead PIs), the Sloan Foundation-Deep Carbon Observatory (Grant 2014–3–01, Kelemen PI), the National Science Foundation (NSF-EAR–1516300, Kelemen lead PI), NASA–Astrobiology Institute (NNA15BB02A, Templeton PI), the German Research Foundation (DFG: KO 1723/21–1, Koepke PI), the Japanese Society for the Promotion of Science (JSPS no:16H06347, Michibayashi PI; and KAKENHI 16H02742, Takazawa PI), the European Research Council (Adv: no.669972; Jamveit PI), the Swiss National Science Foundation (SNF:20FI21_163,073, Früh–Green PI), JAMSTEC, the TAMU–JR Science Operator, and contributions from the Sultanate of Oman Ministry of Regional Municipalities and Water Resources, the Oman Public Authority of Mining, Sultan Qaboos University, CRNS–Univ. Montpellier II, Columbia University of New York, and the University of Southampton. K.W is grateful for receiving the National Science Council, Taiwan (NSC-CDA-107-2628-M-001-006-MY4) and Academia Sinica, Taiwan (AS-CDA-107-M01) funds. F.K.'s participation in shipboard and onsite logging was supported by The Institute of earth science Academia Sinica, Taiwan and by the research grants awarded to K. Michibayashi by the Japan Society for the Promotion of Science (Kiban-B 16340151, Kiban-B 19340148 and Kiban-A 22244062).

References

- Abily, B., & Ceuleneer, G. (2013). The dunitic mantle-crust transition zone in the Oman ophiolite: Residue of melt-rock interaction, cumulates from high-MgO melts, or both? *Geology*, *41*(1), 67–70. <https://doi.org/10.1130/G33351.1>
- Abily, B., Ceuleneer, G., & Launeau, P. (2011). Synmagmatic normal faulting in the lower oceanic crust: Evidence from the Oman ophiolite. *Geology*, *39*(4), 391–394. <https://doi.org/10.1130/g31652.1>
- Abily, B., Ceuleneer, G., Rospabé, M., Kaczmarek, M. A., Python, M., Grégoire, M., et al. (2021). Ocean crust accretion along a high-temperature detachment fault in the Oman ophiolite: A structural and petrological study of the bahla massif. *Tectonophysics*, *229*160. <https://doi.org/10.1016/j.tecto.2021.229160>
- Agranier, A., & Lee, C. T. A. (2007). Quantifying trace element disequilibria in mantle xenoliths and abyssal peridotites. *Earth and Planetary Science Letters*, *257*(1–2), 290–298. <https://doi.org/10.1016/j.epsl.2007.02.041>
- Amri, I., Benoit, M., & Ceuleneer, G. (1996). Tectonic setting for the Genesis of oceanic plagiogranites: Evidence from a paleo-spreading structure in the Oman ophiolite. *Earth and Planetary Science Letters*, *139*(1–2), 177–194. [https://doi.org/10.1016/0012-821x\(95\)00233-3](https://doi.org/10.1016/0012-821x(95)00233-3)
- Asimow, P. D., Hirschmann, M. M., & Stolper, E. M. (2001). Calculation of peridotite partial melting from thermodynamic models of minerals and melts, IV. Adiabatic decompression and the composition and mean properties of mid-ocean ridge basalts. *Journal of Petrology*, *42*(5), 963–998. <https://doi.org/10.1093/ptrology/42.5.963>
- Barrat, J. A., Zanda, B., Moynier, F., Bollinger, C., Liorzou, C., & Bayon, G. (2012). Geochemistry of CI chondrites: Major and trace elements, and Cu and Zn isotopes. *Geochimica et Cosmochimica Acta*, *83*, 79–92. <https://doi.org/10.1016/j.gca.2011.12.011>
- Batanova, V. G., & Savelieva, G. N. (2009). Melt migration in the mantle beneath spreading zones and formation of replacive dunites: A review. *Russian Geology and Geophysics*, *50*(9), 763–778. <https://doi.org/10.1016/j.rgg.2009.08.008>
- Batanova, V. G., Suhr, G., & Sobolev, A. V. (1998). Origin of geochemical heterogeneity in the mantle peridotites from the bay of islands ophiolite, Newfoundland, Canada: Ion probe study of clinopyroxenes. *Geochimica et Cosmochimica Acta*, *62*(5), 853–866. [https://doi.org/10.1016/S0016-7037\(97\)00384-0](https://doi.org/10.1016/S0016-7037(97)00384-0)
- Bedini, R. M., & Bodinier, J. L. (1999). Distribution of incompatible trace elements between the constituents of spinel peridotite xenoliths: ICP-MS data from the east african rift. *Geochimica et Cosmochimica Acta*, *63*(22), 3883–3900. [https://doi.org/10.1016/S0016-7037\(99\)00154-4](https://doi.org/10.1016/S0016-7037(99)00154-4)
- Beinlich, A., Plümper, O., Boter, E., Müller, I. A., Kourim, F., Ziegler, M., et al. (2020). Ophiolite carbonation: Constraints from listvenite core BT1B, Oman drilling Project. *Journal of Geophysical Research: Solid Earth*, *125*, e2019JB019060. <https://doi.org/10.1029/2019jb019060>
- Benn, K., Nicolas, A., & Reuber, I. (1988). Mantle–Crust transition zone and origin of wehrlitic magmas: Evidence from the Oman ophiolite. *Tectonophysics*, *151*(1–4), 75–85. [https://doi.org/10.1016/0040-1951\(88\)90241-7](https://doi.org/10.1016/0040-1951(88)90241-7)
- Benoit, M., Ceuleneer, G., & Polvé, M. (1999). The remelting of hydrothermally altered peridotite at mid-ocean ridges by intruding mantle diapirs. *Nature*, *402*(6761), 514–518. <https://doi.org/10.1038/990073>
- Benoit, M., Polvé, M., & Ceuleneer, G. (1996). Trace element and isotopic characterization of mafic cumulates in a fossil mantle diapir (Oman ophiolite). *Chemical Geology*, *134*(1–3), 199–214. [https://doi.org/10.1016/S0009-2541\(96\)00087-3](https://doi.org/10.1016/S0009-2541(96)00087-3)
- Bodinier, J. L., Vasseur, G., Vernières, J., Dupuy, C., & Fabries, J. (1990). Mechanisms of mantle metasomatism: Geochemical evidence from the Iherz orogenic peridotite. *Journal of Petrology*, *31*(3), 597–628. <https://doi.org/10.1093/ptrology/31.3.597>
- Borisov, A. Y., Ceuleneer, G., Kamenetsky, V. S., Arai, S., Bějina, F., Abily, B., et al. (2012). A new view on the petrogenesis of the Oman ophiolite chro-mitites from microanalyses of chromite-hosted inclusions. *Journal of Petrology*, *53*, 2411–2440. <https://doi.org/10.1093/ptrology/egs054>
- Boudier, F., & Coleman, R. G. (1981). Cross section through the peridotite in the Samail ophiolite, southeastern Oman Mountains. *Journal of Geophysical Research*, *86*, 2573–2592. <https://doi.org/10.1029/JB086iB04p02573>
- Boudier, F., & Nicolas, A. (1995). Nature of the Moho transition zone in the Oman ophiolite. *Journal of Petrology*, *36*(3), 777–796. <https://doi.org/10.1093/ptrology/36.3.777>

- Braun, M. G., & Kelemen, P. B. (2002). Dunite distribution in the Oman ophiolite: Implications for melt flux through porous dunite conduits. *Geochemistry, Geophysics, Geosystems*, 3(11), 1–21. <https://doi.org/10.1029/2001gc000289>
- Ceuleneer, G. (1991). Evidence for a paleo-spreading center in the Oman ophiolite: Mantle structures in the Maqsd area. In *Ophiolite genesis and evolution of the oceanic lithosphere* (pp. 147–173). Springer. https://doi.org/10.1007/978-94-011-3358-6_9
- Ceuleneer, G., Monneréau, M., & Amri, I. (1996). Thermal structure of a fossil mantle diapir inferred from the distribution of mafic cumulates. *Nature*, 379(6561), 149–153. <https://doi.org/10.1038/379149a0>
- Ceuleneer, G., & Nicolas, A. (1985). Structures in podiform chromite from the Maqsd district (Samail ophiolite, Oman). *Mineralium Deposita*, 20(3), 177–184. <https://doi.org/10.1007/BF00204562>
- Ceuleneer, G., Nicolas, A., & Boudier, F. (1988). Mantle flow patterns at an oceanic spreading centre: The Oman peridotites record. *Tectonophysics*, 151(1–4), 1–26. [https://doi.org/10.1016/0040-1951\(88\)90238-7](https://doi.org/10.1016/0040-1951(88)90238-7)
- Clénet, H., Ceuleneer, G., Pinet, P., Abily, B., Daydou, Y., Harris, E., et al. (2010). Thick sections of layered ultramafic cumulates in the Oman ophiolite revealed by an airborne hyperspectral survey: Petrogenesis and relationship to mantle diapirism. *Lithos*, 114(3–4), 265–281. <https://doi.org/10.1016/j.lithos.2009.09.002>
- Collier, M. L., & Kelemen, P. B. (2010). The case for reactive crystallization at mid-ocean ridges. *Journal of Petrology*, 51(9), 1913–1940. <https://doi.org/10.1093/petrology/egq043>
- Dalton, H. B., Scott, J. M., Liu, J., Waight, T. E., Pearson, D. G., Brenna, M., & Palin, J. M. (2017). Diffusion-zoned pyroxenes in an isotopically heterogeneous mantle lithosphere beneath the Dunedin Volcanic Group, New Zealand, and their implications for intraplate alkaline magma sources. *Lithosphere*, 9(3), 463–475. <https://doi.org/10.1130/L631.1>
- de Obeso, J. C., & Kelemen, P. B. (2018). Fluid rock interactions on residual mantle peridotites overlain by shallow oceanic limestones: Insights from Wadi Fins, Sultanate of Oman. *Chemical Geology*, 498, 139–149. <https://doi.org/10.1016/j.chemgeo.2018.09.022>
- Dick, H. J., & Natland, J. H. (1996). Late-stage melt evolution and transport in the shallow mantle beneath the East Pacific Rise. In *Proceedings-ocean drilling Program scientific results* (pp. 103–134). National Science Foundation. <https://doi.org/10.2973/odp.proc.sr.147.007.1996>
- Dick, H. J. B. (1989). Abyssal peridotites, very slow spreading ridges and ocean ridge magmatism. *Geological Society, London, Special Publications*, 42(1), 71–105. <https://doi.org/10.1144/GSL.SP.1989.042.01.06>
- Dyger, N., Kelemen, P. B., & Liang, Y. (2017). Spatial variations in cooling rate in the mantle section of the Samail ophiolite in Oman: Implications for the formation of lithosphere at mid-ocean ridges. *Earth and Planetary Science Letters*, 465, 134–144. <https://doi.org/10.1016/j.epsl.2017.02.038>
- Dyger, N., Liang, Y., & Kelemen, P. B. (2016). Formation of plagioclase lherzolite and associated dunite-harzburgite-lherzolite sequences by multiple episodes of melt percolation and melt-rock reaction: An example from the trinity ophiolite, California, USA. *Journal of Petrology*, 57(4), 815–838. <https://doi.org/10.1093/petrology/egw018>
- Elthon, D. (1979). High magnesia liquids as the parental magma for ocean floor basalts. *Nature*, 278(5704), 514–518. <https://doi.org/10.1038/278514a0>
- Fitzpayne, A., Giuliani, A., Hergt, J., Phillips, D., & Janney, P. (2018). New geochemical constraints on the origins of MARID and PIC rocks: Implications for mantle metasomatism and mantle-derived potassic magmatism. *Lithos*, 318, 478–493. <https://doi.org/10.1016/j.lithos.2018.08.036>
- Frey, F. A., Green, D. H., & Roy, S. D. (1978). Integrated models of basalt petrogenesis: A study of quartz tholeiites to olivine melilitites from south eastern Australia utilizing geochemical and experimental petrological data. *Journal of Petrology*, 19(3), 463–513. <https://doi.org/10.1093/petrology/19.3.463>
- Gerbert-Gaillard, L. (2002). *Caractérisation géochimique des péridotites de l'ophiolite d'Oman: Processus magmatiques aux limites lithosphère/asthénosphère* (p. 238). PhD Thesis Université Montpellier II - Sciences et Techniques du Languedoc.
- Girardeau, J., Monnier, C., Le Mée, L., & Quatrevaux, F. (2002). The wuqbah peridotite, central Oman ophiolite: Petrological characteristics of the mantle in a fossil overlapping ridge setting. *Marine Geophysical Researches*, 23(1), 43–56. <https://doi.org/10.1023/A:1021297614067>
- Glennie, K., Boeuf, M. G. A., Hughes Clarke, M. W., Moody-Stuart, M., Pilaar, W. F. H., & Reinhardt, B. M. (1974). The geology of the Oman Mountains. *Verhandelingen van het Koninklijk Nederlands Geologisch Mijnbouwkundig Genootschap*, 31, 423.
- Godard, M., Bodinier, J. L., & Vasseur, G. (1995). Effects of mineralogical reactions on trace element redistributions in mantle rocks during percolation processes: A chromatographic approach. *Earth and Planetary Science Letters*, 133(3), 449–462. [https://doi.org/10.1016/0012-821X\(95\)00104-K](https://doi.org/10.1016/0012-821X(95)00104-K)
- Godard, M., Bosch, D., & Einaudi, F. (2006). A MORB source for low-Ti magmatism in the Semail ophiolite. *Chemical Geology*, 234(1–2), 58–78. <https://doi.org/10.1016/j.chemgeo.2006.04.005>
- Godard, M., Jousset, D., & Bodinier, J. L. (2000). Relationships between geochemistry and structure beneath a palaeo-spreading centre: A study of the mantle section in the Oman ophiolite. *Earth and Planetary Science Letters*, 180(1–2), 133–148. [https://doi.org/10.1016/S0012-821X\(00\)00149-7](https://doi.org/10.1016/S0012-821X(00)00149-7)
- Godard, M., Lagabrielle, Y., Alard, O., & Harvey, J. (2008). Geochemistry of the highly depleted peridotites drilled at ODP Sites 1272 and 1274 (Fifteen-Twenty Fracture Zone, Mid-Atlantic Ridge): Implications for mantle dynamics beneath a slow spreading ridge. *Earth and Planetary Science Letters*, 267(3–4), 410–425. <https://doi.org/10.1016/j.epsl.2007.11.058>
- Grégoire, M., McInnes, B. I., & O'Reilly, S. Y. (2001). Hydrous metasomatism of oceanic sub-arc mantle, Ithir, Papua New Guinea: Part 2. Trace element characteristics of slab-derived fluids. *Lithos*, 59(3), 91–108. [https://doi.org/10.1016/S0024-4937\(01\)00058-5](https://doi.org/10.1016/S0024-4937(01)00058-5)
- Gruau, G., Bernard-Griffiths, J., & Lécuyer, C. (1998). The origin of U-shaped rare Earth patterns in ophiolite peridotites: Assessing the role of secondary alteration and melt/rock reaction. *Geochimica et Cosmochimica Acta*, 62(21–22), 3545–3560. [https://doi.org/10.1016/S0016-7037\(98\)00250-6](https://doi.org/10.1016/S0016-7037(98)00250-6)
- Hanghøj, K., Kelemen, P. B., Hassler, D., & Godard, M. (2010). Composition and Genesis of depleted mantle peridotites from the Wadi Tayin Massif, Oman Ophiolite; major and trace element geochemistry, and Os isotope and PGE systematics. *Journal of Petrology*, 51(1–2), 201–227. <https://doi.org/10.1093/petrology/egp077>
- Hauri, E. H., & Hart, S. R. (1995). Correction to 'constraints on melt migration from mantle plumes: A trace element study of peridotite xenoliths from savai'i, Western Samoa. *Journal of Geophysical Research*, 100. <https://doi.org/10.1029/95jb00157>
- Hodel, F., Macouin, M., Trindade, R. I. F., Triantafyllou, A., Ganne, J., Chavagnac, V., et al. (2018). Fossil black smoker yields oxygen isotopic composition of Neoproterozoic seawater. *Nature Communications*, 9(1), 1–7. <https://doi.org/10.1038/s41467-018-03890-w>
- Hopson, C. A., Coleman, R. G., Gregory, R. T., Pallister, J. S., & Bailey, E. H. (1981). Geologic section through the Samail ophiolite and associated rocks along a Muscat-Ibra transect, southeastern Oman Mountains. *Journal of Geophysical Research*, 86, 2527–2544. <https://doi.org/10.1029/jb086ib04p02527>
- Jagoutz, E., Palme, H., Baddenhausen, H., Blum, K., Cendales, M., Dreibus, G., et al. (1979). The abundances of major, minor and trace elements in the Earth's mantle as derived from primitive ultramafic nodules. *Proceedings of the Lunar and Planetary Science Conference*, 10, 2031–2050.

- Johnson, K. T., Dick, H. J., & Shimizu, N. (1990). Melting in the oceanic upper mantle: An ion microprobe study of diopsides in abyssal peridotites. *Journal of Geophysical Research*, *95*, 2661–2678. <https://doi.org/10.1029/JB095iB03p02661>
- Johnson, K. T., & Dick, H. J. B. (1992). Open system melting and temporal and spatial variation of peridotite and basalt at the Atlantis II fracture zone. *Journal of Geophysical Research*, *97*, 9219–9241. <https://doi.org/10.1029/92jb00701>
- Jousselin, D., & Nicolas, A. (2000). The Moho transition zone in the Oman ophiolite-relation with wehrlites in the crust and dunites in the mantle. *Marine Geophysical Researches*, *21*(3–4), 229–241. <https://doi.org/10.1023/A:1026733019682>
- Jousselin, D., Nicolas, A., & Boudier, F. (1998). Detailed mapping of a mantle diapir below a paleo-spreading center in the Oman ophiolite. *Journal of Geophysical Research*, *103*, 18153–18170. <https://doi.org/10.1029/98JB01493>
- Kanke, N., & Takazawa, E. (2014). A kilometre-scale highly refractory harzburgite zone in the mantle section of the northern Oman ophiolite (fizh block): Implications for flux melting of oceanic lithospheric mantle. *Geological Society, London, Special Publications*, *392*(1), 229–246. <https://doi.org/10.1144/SP392.12>
- Kelemen, P. B. (1990). Reaction between ultramafic rock and fractionating basaltic magma I. phase relations, the origin of calc-alkaline magma series, and the formation of discordant dunite. *Journal of Petrology*, *31*, 51–98. <https://doi.org/10.1093/petrology/31.1.51>
- Kelemen, P. B., Dick, H. J. B., & Quick, J. E. (1992). Formation of harzburgite by pervasive melt/rock reaction in the upper mantle. *Nature*, *358*, 635–641. <https://doi.org/10.1038/358635a0>
- Kelemen, P. B., & Ghiorso, M. S. (1986). Assimilation of peridotite in zoned calc-alkaline plutonic complexes: Evidence from the big jim complex, Washington cascades. *Contributions to Mineralogy and Petrology*, *94*(1), 12–28. <https://doi.org/10.1007/bf00371222>
- Kelemen, P. B., Hart, S. R., & Bernstein, S. (1998). Silica enrichment in the continental upper mantle via melt/rock reaction. *Earth and Planetary Science Letters*, *164*(1–2), 387–406. [https://doi.org/10.1016/S0012-821X\(98\)00233-7](https://doi.org/10.1016/S0012-821X(98)00233-7)
- Kelemen, P. B., Hirth, G., Shimizu, N., Spiegelman, M., & Dick, H. J. (1997). A review of melt migration processes in the adiabatically upwelling mantle beneath oceanic spreading ridges. *Philosophical Transactions of the Royal Society of London, Series A: Mathematical, Physical and Engineering Sciences*, *355*(1723), 283–318. <https://doi.org/10.1098/rsta.1997.0010>
- Kelemen, P. B., Matter, J. M., Teagle, D. A. H., & Coggon, J. A., & Oman Drilling Project Science Team. (2020a). Site CM1: Layered gabbros, crustal ultramafic rocks, and mantle harzburgite. In P. B. Kelemen, J. M. Matter, D. A. H. Teagle, J. A. Coggon, et al. (Eds.), *Proceedings of the Oman drilling Project*. International Ocean Discovery Program.
- Kelemen, P. B., Matter, J. M., Teagle, D. A. H., & Coggon, J. A., & Oman Drilling Project Science Team. (2020b). Site CM2: Crust-mantle transition zone and into upper mantle. In P. B. Kelemen, J. M. Matter, D. A. H. Teagle, J. A. Coggon, et al. (Eds.), *Proceedings of the Oman drilling Project: College station, TX (international ocean discovery program)*. in press. <https://doi.org/10.14379/OmanDP.proc.2020>
- Kelemen, P. B., Matter, J. M., Teagle, D. A. H., & Coggon, J. A., & Oman Drilling Project Science Team. (2020c). Methods and explanatory notes. In P. B. Kelemen, J. M. Matter, D. A. H. Teagle, J. A. Coggon, et al. (Eds.), *Proceedings of the Oman drilling Project*. International Ocean Discovery Program.
- Kelemen, P. B., Shimizu, N., & Dunn, T. (1993). Relative depletion of niobium in some arc magmas and the continental crust: Partitioning of K, Nb, La and Ce during melt/rock reaction in the upper mantle. *Earth and Planetary Science Letters*, *120*(3–4), 111–134. [https://doi.org/10.1016/0012-821X\(93\)90234-Z](https://doi.org/10.1016/0012-821X(93)90234-Z)
- Kelemen, P. B., Shimizu, N., & Salters, V. J. (1995). Extraction of mid-ocean-ridge basalt from the upwelling mantle by focused flow of melt in dunite channels. *Nature*, *375*(6534), 747–753. <https://doi.org/10.1038/375747a0>
- Khedr, M. Z., Arai, S., Python, M., & Tamura, A. (2014). Chemical variations of abyssal peridotites in the central Oman ophiolite: Evidence of oceanic mantle heterogeneity. *Gondwana Research*, *25*(3), 1242–1262. <https://doi.org/10.1016/j.gr.2013.05.010>
- Koga, K. T., Kelemen, P. B., & Shimizu, N. (2001). Petrogenesis of the crust-mantle transition zone and the origin of lower crustal wehrlite in the Oman ophiolite. *Geochemistry, Geophysics, Geosystems*, *2*(9). <https://doi.org/10.1029/2000gc000132>
- Kogiso, T., Tatsumi, Y., & Nakano, S. (1997). Trace element transport during dehydration processes in the subducted oceanic crust: 1. Experiments and implications for the origin of ocean island basalts. *Earth and Planetary Science Letters*, *148*(1–2), 193–205. [https://doi.org/10.1016/S0012-821X\(97\)00018-6](https://doi.org/10.1016/S0012-821X(97)00018-6)
- Kourim, F., Bodinier, J. L., Alard, O., Bendaoud, A., Vauchez, A., & Dauria, J. M. (2014). Nature and evolution of the lithospheric mantle beneath the hoggar swell (Algeria): A record from mantle xenoliths. *Journal of Petrology*, *55*(11), 2249–2280. <https://doi.org/10.1093/petrology/egu056>
- Langmuir, C. H., Klein, E. M., & Plank, T. (1992). Petrological systematics of mid-ocean ridge basalts: Constraints on melt generation beneath ocean ridges. *Mantle flow and melt generation at mid-ocean ridges*, *71*, 183–280.
- Leblanc, M., & Ceuleneer, G. (1991). Chromite crystallization in a multicellular magma flow: Evidence from a chromitite dike in the Oman ophiolite. *Lithos*, *27*, 231–257. [https://doi.org/10.1016/0024-4937\(91\)90002-3](https://doi.org/10.1016/0024-4937(91)90002-3)
- Lee, C. T. A., Harbert, A., & Leeman, W. P. (2007). Extension of lattice strain theory to mineral/mineral rare-Earth element partitioning: An approach for assessing disequilibrium and developing internally consistent partition coefficients between olivine, orthopyroxene, clinopyroxene and basaltic melt. *Geochimica et Cosmochimica Acta*, *71*(2), 481–496. <https://doi.org/10.1016/j.gca.2006.09.014>
- Le Mée, L., Girardeau, J., & Monnier, C. (2004). Mantle segmentation along the Oman ophiolite fossil mid-ocean ridge. *Nature*, *432*(7014), 167–172. <https://doi.org/10.1038/nature03075>
- Lippard, S. J., Shelton, A. W., & Gass, I. G. (1986). *The Ophiolite of Northern Oman* (Vol. 11). Geological Society London Memoir. 178.
- Lorand, J. P. (1988). Fe-Ni-Cu sulfides in tectonite peridotites from the Maqсад district, Sumail ophiolite, southern Oman: Implications for the origin of the sulfide component in the oceanic upper mantle. *Tectonophysics*, *151*(1–4), 57–73. [https://doi.org/10.1016/0040-1951\(88\)90240-5](https://doi.org/10.1016/0040-1951(88)90240-5)
- Lorand, J.-P., & Ceuleneer, G. (1989). Silicate and base-metal sulfide inclusions in chromites from the Maqсад area (Oman ophiolite, gulf of Oman): A model for entrapment. *Lithos*, *22*, 173–190. [https://doi.org/10.1016/0024-4937\(89\)90054-6](https://doi.org/10.1016/0024-4937(89)90054-6)
- Malvoisin, B. (2015). Mass transfer in the oceanic lithosphere: Serpentinization is not isochemical. *Earth and Planetary Science Letters*, *430*, 75–85. <https://doi.org/10.1016/j.epsl.2015.07.043>
- McKenzie, D., & O'Nions, R. K. (1991). Partial melt distributions from inversion of rare Earth element concentrations. *Journal of Petrology*, *32*(5), 1021–1091. <https://doi.org/10.1093/petrology/32.5.1021>
- Monnier, C., Girardeau, J., Le Mée, L., & Polvé, M. (2006). Along-ridge petrological segmentation of the mantle in the Oman ophiolite. *Geochemistry, Geophysics, Geosystems*, *7*(11). <https://doi.org/10.1029/2006GC001320>
- Morgan, Z., Liang, Y., & Kelemen, P. B. (2008). Significance of the concentration gradients associated with dunite bodies in the Josephine and Trinity ophiolites. *Geochemistry, Geophysics, Geosystems*, *9*(7). <https://doi.org/10.1029/2008GC001954>
- Navon, O., & Stolper, E. (1987). Geochemical consequences of melt percolation: The upper mantle as a chromatographic column. *The Journal of Geology*, *95*(3), 285–307. <https://doi.org/10.1086/629131>
- Nicolas, A. (2012). *Structures of Ophiolites and Dynamics of Oceanic Lithosphere* (Vol. 4). Springer Science & Business Media.

- Nicolas, A., & Boudier, F. (1995). Mapping oceanic ridge segments in Oman ophiolite. *Journal of Geophysical Research*, *100*, 6179–6197. <https://doi.org/10.1029/94jb01188>
- Nicolas, A., & Boudier, F. (2008). Large shear zones with no relative displacement. *Terra Nova*, *20*(3), 200–205. <https://doi.org/10.1111/j.1365-3121.2008.00806.x>
- Nicolas, A., Boudier, F., Ildefonse, B., & Ball, E. (2000). Accretion of Oman and United Arab Emirates ophiolite—discussion of a new structural map. *Marine Geophysical Researches*, *21*(3–4), 147–180. <https://doi.org/10.1023/A:1026769727917>
- Nicolas, A., Ceuleneer, G., Boudier, F., & Misseri, M. (1988). Structural mapping in the Oman ophiolites: Mantle diapirism along an oceanic ridge. *Tectonophysics*, *151*(1–4), 27–56. [https://doi.org/10.1016/0040-1951\(88\)90239-9](https://doi.org/10.1016/0040-1951(88)90239-9)
- Nicolle, M., Jousset, D., Reisberg, L., Bosch, D., & Stephan, A. (2016). Major and trace element and Sr and Nd isotopic results from mantle diapirs in the Oman ophiolite: Implications for off-axis magmatic processes. *Earth and Planetary Science Letters*, *437*, 138–149. <https://doi.org/10.1016/j.epsl.2015.12.005>
- Niu, Y. (1997). Mantle melting and melt extraction processes beneath ocean ridges: Evidence from abyssal peridotites. *Journal of Petrology*, *38*(8), 1047–1074. <https://doi.org/10.1093/ptro/38.8.1047>
- Niu, Y. (2004). Bulk-rock major and trace element compositions of abyssal peridotites: Implications for mantle melting, melt extraction and post-melting processes beneath mid-ocean ridges. *Journal of Petrology*, *45*, 2423–2458. <https://doi.org/10.1093/ptro/egh068>
- O'Hara, M. J. (1965). Primary magmas and the origin of basalts. *Scottish Journal of Geology*, *1*(1), 19–40. <https://doi.org/10.1144/sjg01010019>
- Oliveira, B., Afonso, J. C., & Tilhac, R. (2020). A disequilibrium reactive transport model for mantle magmatism. *Journal of Petrology*. <https://doi.org/10.1093/ptrology/egaa067>
- Parkinson, I. J., & Pearce, J. A. (1998). Peridotites from the izu–bonin–mariana forearc (ODP Leg 125): Evidence for mantle melting and melt–mantle interaction in a supra-subduction zone setting. *Journal of Petrology*, *39*(9), 1577–1618. <https://doi.org/10.1093/ptro/39.9.1577>
- Paulick, H., Bach, W., Godard, M., De Hoog, J. C. M., Suhr, G., & Harvey, J. (2006). Geochemistry of abyssal peridotites (Mid-Atlantic Ridge, 15° 20' N, ODP Leg 209): Implications for fluid/rock interaction in slow spreading environments. *Chemical Geology*, *234*(3–4), 179–210. <https://doi.org/10.1016/j.chemgeo.2006.04.011>
- Prinzhofer, A., & Allègre, C. J. (1985). Residual peridotites and the mechanisms of partial melting. *Earth and Planetary Science Letters*, *74*(2–3), 251–265. [https://doi.org/10.1016/0012-821X\(85\)90025-1](https://doi.org/10.1016/0012-821X(85)90025-1)
- Python, M., & Ceuleneer, G. (2003). Nature and distribution of dykes and related melt migration structures in the mantle section of the Oman ophiolite. *Geochemistry, Geophysics, Geosystems*, *4*(7). <https://doi.org/10.1029/2002GC000354>
- Python, M., Ceuleneer, G., & Arai, S. (2008). Chromian spinels in mafic–ultramafic mantle dykes: Evidence for a two-stage melt production during the evolution of the Oman ophiolite. *Lithos*, *106*(1–2), 137–154. <https://doi.org/10.1016/j.lithos.2008.07.001>
- Quick, J. E. (1981a). The origin and significance of large, tabular dunite bodies in the Trinity peridotite, northern California. *Contributions to Mineralogy and Petrology*, *78*(4), 413–422. <https://doi.org/10.1007/BF00375203>
- Quick, J. E. (1981b). Petrology and petrogenesis of the trinity peridotite, an upper mantle diapir in the eastern Klamath mountains, northern California. *Journal of Geophysical Research*, *86*, 11837–11863. <https://doi.org/10.1029/JB086iB12p11837>
- Rabinowicz, M., Ceuleneer, G., & Nicolas, A. (1987). Melt segregation and flow in mantle diapirs below spreading centers: Evidence from the Oman ophiolite. *Journal of Geophysical Research*, *92*, 3475–3486. <https://doi.org/10.1029/JB092iB05p03475>
- Rioux, M., Bowring, S., Kelemen, P., Gordon, S., Dudás, F., & Miller, R. (2012). Rapid crustal accretion and magma assimilation in the Oman-UAE ophiolite: High precision U–Pb zircon geochronology of the gabbroic crust. *Journal of Geophysical Research*, *117*. <https://doi.org/10.1029/2012JB009273>
- Rioux, M., Bowring, S., Kelemen, P., Gordon, S., Miller, R., & Dudás, F. (2013). Tectonic development of the Semail ophiolite: High-precision U–Pb zircon geochronology and Sm–Nd isotopic constraints on crustal growth and emplacement. *Journal of Geophysical Research: Solid Earth*, *118*(5), 2085–2101. <https://doi.org/10.1002/jgrb.50139>
- Rioux, M., Garber, J., Bauer, A., Bowring, S., Searle, M., Kelemen, P., & Hacker, B. (2016). Synchronous formation of the metamorphic sole and igneous crust of the Semail ophiolite: New constraints on the tectonic evolution during ophiolite formation from high-precision U–Pb zircon geochronology. *Earth and Planetary Science Letters*, *451*, 185–195. <https://doi.org/10.1016/j.epsl.2016.06.051>
- Rollinson, H., & MameriBarry, L. T. (2018). Polyminerale inclusions in mantle chromitites from the Oman ophiolite indicate a highly magnesian parental melt. *Lithos*, *310–311*, 381–391. <https://doi.org/10.1016/j.lithos.2018.04.024>
- Rospabé, M. (2018). Etude pétrologique, géochimique et structurale de la zone de transition dunitique dans l'ophio-lite d'Oman: Identification des processus pétrogénétiques à l'interface manteau/croûte (Doctoral dissertation, Université Paul Sabatier, in Toulouse III (Ed.)).
- Rospabé, M., Benoit, M., & Candaudap, F. (2018a). Determination of trace element mass fractions in ultramafic rocks by HR-ICP-MS: A combined approach using a direct digestion/dilution method and preconcentration by coprecipitation. *Geostandards and Geoanalytical Research*, *42*(1), 115–129. <https://doi.org/10.1111/ggr.12181>
- Rospabé, M., Benoit, M., Ceuleneer, G., Hodel, F., & Kaczmarek, M. A. (2018b). Extreme geochemical variability through the dunitic transition zone of the Oman ophiolite: Implications for melt/fluid-rock reactions at moHo level beneath oceanic spreading centers. *Geochimica et Cosmochimica Acta*, *234*, 1–23. <https://doi.org/10.1016/j.gca.2018.05.012>
- Rospabé, M., Benoit, M., Ceuleneer, G., Kaczmarek, M. A., & Hodel, F. (2019a). Melt hybridization and metasomatism triggered by syn-magmatic faults within the Oman ophiolite: A clue to understand the Genesis of the dunitic mantle-crust transition zone. *Earth and Planetary Science Letters*, *516*, 108–121. <https://doi.org/10.1016/j.epsl.2019.04.004>
- Rospabé, M., Ceuleneer, G., Benoit, M., Abily, B., & Pinet, P. (2017). Origin of the dunitic mantle-crust transition zone in the Oman ophiolite: The interplay between percolating magmas and high-temperature hydrous fluids. *Geology*, *45*(5), 471–474. <https://doi.org/10.1130/G38778.1>
- Rospabé, M., Ceuleneer, G., Benoit, M., & Kaczmarek, M. A. (2020). Composition gradients in silicate inclusions in chromites from the dunitic mantle-crust transition (Oman ophiolite) reveal high temperature fluid-melt-rock interaction controlled by faulting. *Ophioliti. An international journal on ophiolites and oceanic lithosphere*, *45*(2), 103–114. <https://doi.org/10.4454/ofioliti.v45i2.534>
- Rospabé, M., Ceuleneer, G., Le Guluche, V., Benoit, M., & Kaczmarek, M. A. (2021). The chicken and egg dilemma linking dunites and chromitites in the mantle-crust transition zone beneath oceanic spreading centres: A case study of chromite-hosted silicate inclusions in dunites formed at the top of a mantle diapir (Oman ophiolite). *Journal of Petrology*.
- Sauter, D., Werner, P., Ceuleneer, G., Manatschal, G., Rospabé, M., Tugend, J., & Ulrich, M. (2021). Sub-axial deformation in oceanic lower crust: Insights from seismic reflection profiles in the Enderby Basin and comparison with the Oman ophiolite. *Earth and Planetary Science Letters*, *554*, 116698. <https://doi.org/10.1016/j.epsl.2020.116698>
- Schiano, P., Clochiatti, R., Lorand, J.-P., Massare, D., & DeloucheChaussidon, E. M. (1997). Primitive basaltic melts included in podiform chromites from the Oman Ophiolite. *Earth and Planetary Science Letters*, *146*, 489–497. [https://doi.org/10.1016/s0012-821x\(96\)00254-3](https://doi.org/10.1016/s0012-821x(96)00254-3)

- Searle, M. P., & Malpas, J. (1980). Structure and metamorphism of rocks beneath the Semail ophiolite of Oman and their significance in ophiolite obduction. *Earth and Environmental Science Transactions of the Royal Society of Edinburgh*, 71(4), 247–262. <https://doi.org/10.1017/S0263593300013614>
- Smewing, J. D. (1981). Mixing characteristics and compositional differences in mantle-derived melts beneath spreading axes: Evidence from cyclically layered rocks in the ophiolite of North Oman. *Journal of Geophysical Research*, 86(B4), 2645–2659. <https://doi.org/10.1029/JB086iB04p02645>
- Snow, J. E., & Dick, H. J. (1995). Pervasive magnesium loss by marine weathering of peridotite. *Geochimica et Cosmochimica Acta*, 59(20), 4219–4236. [https://doi.org/10.1016/0016-7037\(95\)00239-V](https://doi.org/10.1016/0016-7037(95)00239-V)
- Spiegelman, M., & Kelemen, P. B. (2003). Extreme chemical variability as a consequence of channelized melt transport. *Geochemistry, Geophysics, Geosystems*, 4(7). <https://doi.org/10.1029/2002gc000336>
- Sun, C., & Liang, Y. (2014). An assessment of subsolidus re-equilibration on REE distribution among mantle minerals olivine, orthopyroxene, clinopyroxene, and garnet in peridotites. *Chemical Geology*, 372, 80–91. <https://doi.org/10.1016/j.chemgeo.2014.02.014>
- Sun, S. S., & McDonough, W. F. (1989). Chemical and isotopic systematics of oceanic basalts: Implications for mantle composition and processes. *Geological Society, London, Special Publications*, 42(1), 313–345. <https://doi.org/10.1144/gsl.sp.1989.042.01.19>
- Takazawa, E., Frey, F. A., Shimizu, N., Obata, M., & Bodinier, J. L. (1992). Geochemical evidence for melt migration and reaction in the upper mantle. *Nature*, 359(6390), 55–58. <https://doi.org/10.1038/359055a0>
- Takazawa, E., Okayasu, T., & Satoh, K. (2003). Geochemistry and origin of the basal lherzolites from the northern Oman ophiolite (northern Fizh block). *Geochemistry, Geophysics, Geosystems*, 4(2). <https://doi.org/10.1029/2001GC000232>
- Tilton, G. R., Hopson, C. A., & Wright, J. E. (1981). Uranium-lead isotopic ages of the Semail ophiolite, Oman, with applications to Tethyan ocean ridge tectonics. *Journal of Geophysical Research*, 86, 2763–2775. <https://doi.org/10.1029/JB086iB04p02763>
- Tippit, P. R., Pessagno, E. A., & Smewing, J. D. (1981). The biostratigraphy of sediments in the volcanic unit of the Semail ophiolite. *Journal of Geophysical Research*, 86(B4), 2756–2762. <https://doi.org/10.1029/JB086iB04p02756>
- Tommasi, A., & Vauchez, A. (2015). Heterogeneity and anisotropy in the lithospheric mantle. *Tectonophysics*, 661, 11–37. <https://doi.org/10.1016/j.tecto.2015.07.026>
- Vauchez, A., Dineur, F., & Rudnick, R. (2005). Microstructure, texture and seismic anisotropy of the lithospheric mantle above a mantle plume: Insights from the labait volcano xenoliths (Tanzania). *Earth and Planetary Science Letters*, 232(3–4), 295–314. <https://doi.org/10.1016/j.epsl.2005.01.024>
- Vernières, J., Godard, M., & Bodinier, J. L. (1997). A plate model for the simulation of trace element fractionation during partial melting and magma transport in the Earth's upper mantle. *Journal of Geophysical Research*, 102(B11), 24771–24784. <https://doi.org/10.1029/97JB01946>
- Walter, M. J., Sisson, T. W., & Presnall, D. C. (1995). A mass proportion method for calculating melting reactions and application to melting of model upper mantle lherzolite. *Earth and Planetary Science Letters*, 135(1–4), 77–90. [https://doi.org/10.1016/0012-821X\(95\)00148-6](https://doi.org/10.1016/0012-821X(95)00148-6)
- Warren, J. B., & Shimizu, N. (2010). Cryptic variations in abyssal peridotite compositions: Evidence for shallow-level melt infiltration in the oceanic lithosphere. *Journal of Petrology*, 51(1–2), 395–423. <https://doi.org/10.1093/ptrology/egp096>
- Warren, C. J., Parrish, R. R., Waters, D. J., & Searle, M. P. (2005). Dating the geologic history of Oman's Semail ophiolite: Insights from U-Pb geochronology. *Contributions to Mineralogy and Petrology*, 150(4), 403–422. <https://doi.org/10.1007/s00410-005-0028-5>
- Warren, J. M., Shimizu, N., Skaaguchi, C., Dick, H. J. B., & Nakamura, E. (2009). An assessment of upper mantle heterogeneity based on abyssal peridotite isotopic compositions. *Journal of Geophysical Research*, 114, B12203. <https://doi.org/10.1029/2008JB006186>
- Zagrtednov, N. R., Ceuleneer, G., Rospabé, M., Borisova, A. Y., Toplis, M. J., Benoit, M., & Abily, B. (2018). Anatomy of a chromitite dyke in the mantle/crust transition zone of the Oman ophiolite. *Lithos*, 312, 343–357. <https://doi.org/10.1016/j.lithos.2018.05.012>

References From the Supporting Information

- Barth, M. G., Mason, P. R., Davies, G. R., Dijkstra, A. H., & Drury, M. R. (2003). Geochemistry of the othris ophiolite, Greece: Evidence for refertilization? *Journal of Petrology*, 44(10), 1759–1785. <https://doi.org/10.1093/ptrology/egg058>
- Ionov, D. A., Savoyant, L., & Dupuy, C. (1992). Application of the ICP-MS technique to trace element analysis of peridotites and their minerals. *Geostandards Newsletter*, 16(2), 311–315. <https://doi.org/10.1111/j.1751-908X.1992.tb00494.x>
- Rospabé, M., Ceuleneer, G., Granier, N., Arai, S., & Borisova, A. Y. (2019b). Multi-scale development of a stratiform chromite ore body at the base of the dunitic mantle–crust transition zone (Maqsad diapir, Oman ophiolite): The role of repeated melt and fluid influxes. *Lithos*, 350–351, 105235.
- Yokoyama, T., Makishima, A., & Nakamura, E. (1999). Evaluation of the coprecipitation of incompatible trace elements with fluoride during silicate rock dissolution by acid digestion. *Chemical Geology*, 157(3–4), 175–187. [https://doi.org/10.1016/s0009-2541\(98\)00206-x](https://doi.org/10.1016/s0009-2541(98)00206-x)